

MŰSZAKI SZEMLE

47. szám, 2009.

**Szerkesztőbizottság elnöke /
President of Editing Committee**

Dr. Köllő Gábor

**Szerkesztőbizottság tagjai /
Editing Committee**

Dr. Balázs L. György – HU,
Dr. Biró Károly Ágoston – RO,
Dr. Csibi Vencel-József – RO,
Dr. Fedák László – UA,
Dr. Kása Zoltán – RO,
Dr. Kászonyi Gábor – HU,
Dr. Majdik Kornélia – RO,
Dr. Maros Dezső – RO,
Dr. Nagy László – RO,
Dr. Pécs Hajnalka – YU,
Dr. Puskás Ferenc – RO,
Dr. Szalay György – SK,
Dr. Turchany Guy – CH

Kiadja / Editor

Erdélyi Magyar Műszaki
Tudományos Társaság – EMT
Societatea Maghiară Tehnico-Științifică
din Transilvania
Ungarische Technisch-Wissenschaftliche
Gesellschaft in Siebenbürgen
Hungarian Technical Scientific Society
of Transylvania

Felelős kiadó / Managing Editor

Dr. Köllő Gábor

A szerkesztőség címe / Address

Romania
400604 Cluj, Kolozsvár
B-dul 21. Decembrie 1989., nr. 116.
Tel/fax: 40-264-590825, 594042
Levelezési cím: RO – 400750 Cluj, C.P. 1-140.

Nyomda / Printing

Incitato Kft.

ISSN 1454-0746

**Periodical accredited
by the CNCSIS**

CNCSIS által elismert folyóirat

Revistă acreditată de CNCSIS

www.emt.ro

emt@emt.ro

Content – Tartalomjegyzék – Cuprins

Concrete in Fire Tűz hatása a betonra Acțiunea focului asupra betonului György L. BALÁZS, Éva LUBLÓY	3
Stability in Bending and Axial Compression of Steel Members A nyomóerőre és hajlítónyomatékra igénybevett acél tartó stabilitása Stabilitatea barei metalice solicitată la compresiune și încovoiere Ștefan GUȚIU, Gavril KÖLLŐ, Petru MOGA, Cătălin MOGA	11
Thin – Walled Composite Columns Együttdolgozó öszvérkeresztmetszetű oszlopok megvalósítása vékony lemezek segítségével Stâlpi cu secțiune compusă din bare cu pereți subțiri Petru MOGA, Gavril KÖLLŐ, Ștefan GUȚIU, Cătălin MOGA	20
The Influence of Composite Column Slenderness on the Confinement Effect Az együttdolgozó – öszvérkeresztmetszetű oszlopok karcsúságának a hatása a beton keresztirányú alakváltozását gátló jelenség együtthatójára Influența zvelteții stâlpului cu secțiune compozită asupra factorului de confinare Petru MOGA, Gavril KÖLLŐ, Ștefan GUȚIU, Cătălin MOGA	29
Presence of Chloride Ions in Concrete Kloridionok a betonban Ionii de clorid în beton Katalin KOPECSKÓ	35
Vertical Displacements of a Steel-concrete Superstructure, 51m Long, Under the THALYS Train Load, with Speeds Ranging Between 1...110m/s. A THALYS nagysebességű vonat által gerjesztett lehajlások egy öszvérkeresztmetszetű híd hosszában Deformații vertical la un pod de cale ferată cu secțiune mixtă a vând deschiderea de 50m sub acțiunea convoiului THALYS, cu viteze între 1...110m/s Gavril KÖLLŐ, Mircea A. SUCIU	43
Vertical Displacements of a Steel-concrete Railway Superstructure, 51m Long, Under the 250KN Mobile Axle Load, for Speed Ranging Between 1...150m/s. Egy nagysebességű mozgó tengely (P=250kN) által gerjesztett lehajlások egy öszvérkeresztmetszetű híd hosszában Deformații vertical la un pod de cale ferată cu secțiune mixtă având deschiderea de 50m sub acțiunea unei osi mobile (P=250kN), cu viteze între 1...150m/s Mircea A. SUCIU, Gavril KÖLLŐ	50

A kiadvány megjelenését támogatta:



Szülőföld Alap Iroda – Budapest



COMMUNITAS
ALAPÍTVÁNY

Communitas Alapítvány – Kolozsvár

Concrete in Fire

Tűz hatása a betonra

Acțiunea focului asupra betonului

György L. BALÁZS, Éva LUBLÓY

Budapest University of Technology and Economics, Hungary
H-1111 Budapest Műegyetem rakpart balazs@vbt.bme.hu, lubeva@web.de

ÖSSZEFOGLALÓ

Az utóbbi évtizedekben számos épületkatasztrófa igazolta, hogy a tűzterherre való méretezés továbbra is nagy jelentőséggel bír. Tűz esetén szükséges, hogy ismerjük a különböző építőanyagok magas hőmérséklet hatására való viselkedését, illetve a szilárdságuk alakulását (Janson, Boström, 2004). A betonok magas hőmérséklettel szembeni viselkedését jelentős mértékben befolyásolja a cement típusa és a víz-cementtényező és az adalékanyag típusa is (Thielen, 1994). A betonösszetétel tervezése tűzterherre ezért nagy jelentőséget kap és kaphat.

REZUMAT

Catastrofele unor clădiri datorată acțiunii focului justifică luarea în considerare a acestei acțiuni la proiectare. În cazul incendiilor trebuie să cunoaștem comportarea diferitelor materiale de construcții la temperaturi ridicate, modificările intervenite în aceste situații privind rezistența lor. (Jansos, Bostrom, 2004)

Comportarea betoanelor la temperaturi ridicate este influențată de tipul cimentului, de raportul apă-ciment și de materiale de adaos. (Thielen, 1994) De aceea proiectarea compoziției betoanelor rezistente la foc devine foarte importantă în viitor.

SUMMARY

Recent fire cases indicated again the importance of fire research. Fast development of construction technology requires new materials. Initiation and development of fire are strongly influenced by the choice of construction materials. In addition to their mechanical properties, their behaviour in elevated temperature is also of high importance (Janson, Boström, 2004). Residual compressive strength of concrete exposed to high temperatures is influenced by the following factors (Thielen, 1994): water to cement ratio, cement to aggregate ratio, type of aggregate, water content of concrete before exposing it to high temperatures and the fire process. Therefore, mix design and composition of concrete is of high importance for high temperatures.

1. INTRODUCTION

Concrete has excellent properties in regards of fire resistance compared with other materials and can be used to shield other structural materials such as steel (Khoury, Grainger, Sullivan, 1985).

Effects of high temperatures on the mechanical properties of concrete have been investigated as early as the 1940s (Schneider, 1988). In the 1960s and 1970s fire research was mainly directed to study the behaviour of concrete structural elements (Kordina, 1997). There was relatively little information on the concrete properties during and after fire (Waubke, 1973).

During fire the mechanical characteristics of the concrete are changing. During the cooling process concrete is not able to recover its original characteristics. Deterioration of concrete at high temperatures has two forms: (1) local damage in the material itself (*Fig. 1*) and global damage resulting the failure of the elements (*Fig. 2*).

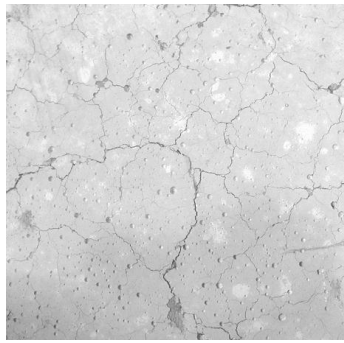


Fig. 1.
Damage of concrete



Fig. 2.
Damage of structure
(<http://www.polizia.ti.ch>)

2. CHEMICAL TRANSFORMATIONS OF CONCRETE

Concrete is a composite material, that consists mainly of mineral aggregates bound by a matrix of hydrated cement paste. The matrix is highly porous and contains a relatively large amount of free water unless artificially dried. When exposed it to high temperatures, concrete undergoes changes in its chemical composition, physical structure and water content (Fig. 3). These changes occur primarily in the hardened cement paste in unsealed conditions (Fig. 4) Such changes are reflected by changes in the physical and mechanical properties of concrete that are associated with temperature increase.

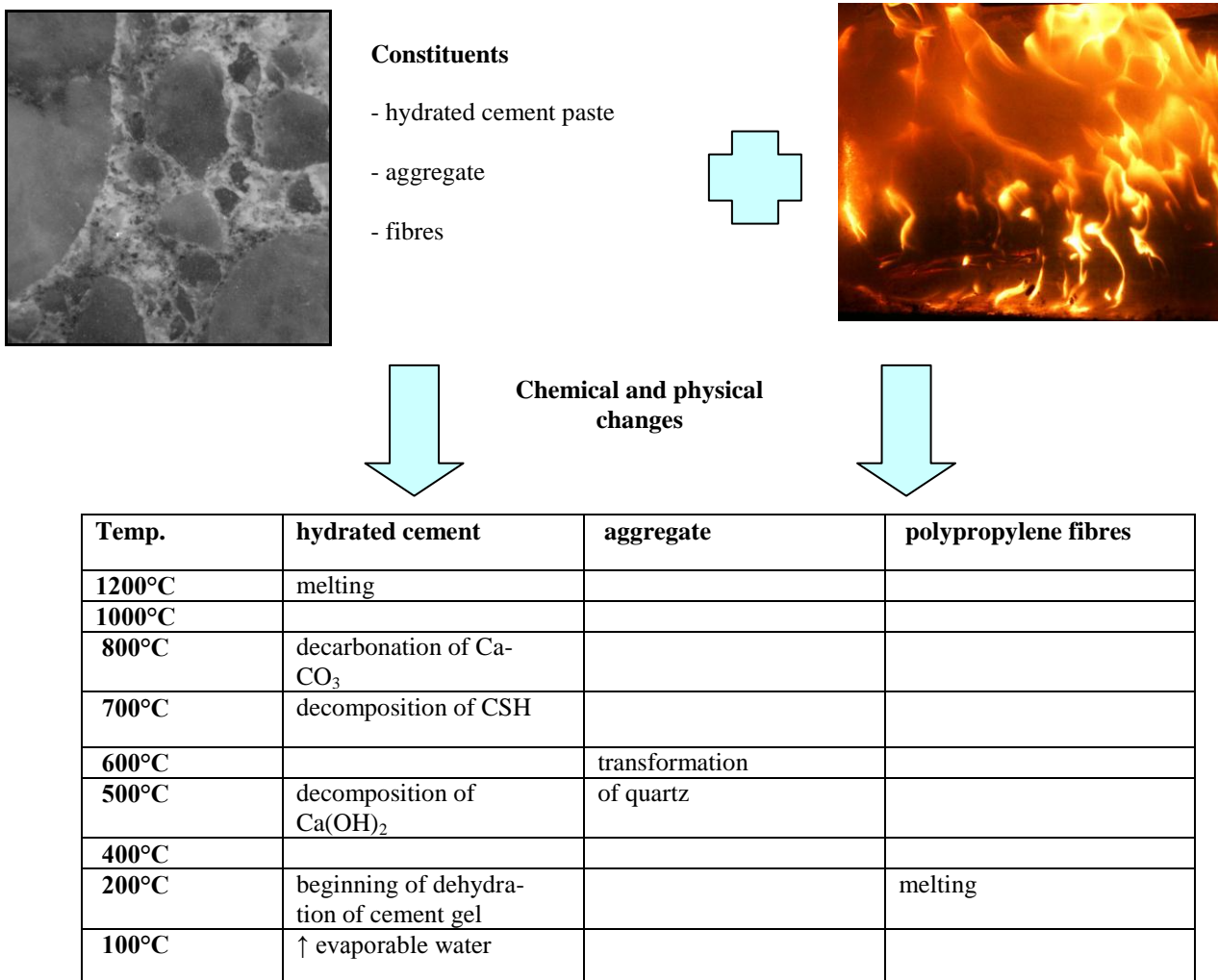


Fig. 3:
Chemical changes of constituents of concrete during fire

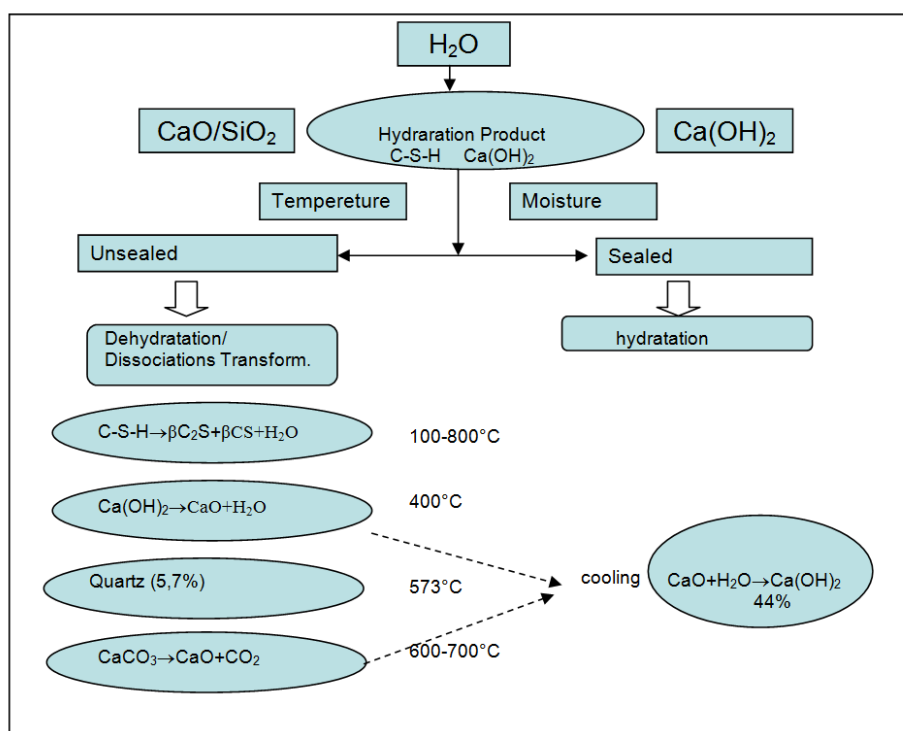


Fig. 4:
The influence of temperature and moisture upon the chemical transformations and hydration products (*fib* bulletin 38, 2007)

Chemical changes can be studied with thermogravimetric analyses (TG/DTG/DTA).

The following chemical transformations can be observed by increase of temperature: Around 100°C the weight loss is caused by water evaporating from the micropores. The decomposition of ettringite ($3\text{CaOAl}_2\text{O}_3 \cdot 3\text{CaSO}_4 \cdot 32\text{H}_2\text{O}$) occurs between 50°C and 110°C. At 200°C there is further dehydration which causes small weight loss. The weight loss with various moisture contents was different till all the pore water and chemically bound water were gone. Further weight loss was not perceptible around 250-300°C (Khoury, Grainger, Sullivan, 1985, Schneider, Wiess, 1977).

During heating the endothermic dehydration of Ca(OH)_2 occurs between the temperatures of 450°C and 550°C ($\text{Ca(OH)}_2 \rightarrow \text{CaO} + \text{H}_2\text{O}\uparrow$) (Schneider, Wiess, 1977). In case of concretes with quartz gravel aggregate another influencing factor is the change of crystal structure of quartz α formation \rightarrow β formation at the temperature of 573°C (Waubke, 1973). This transformation is followed by 5.7% volumetric increase.

Dehydration of calcium-silicate-hydrates were found at the temperature of 700°C (Hinrichsmeyer, 1989, Fig. 3).

3. RESIDUAL COMPRESSIVE STRENGTH OF CONCRETE

Temperature influences are reflected in changes of physical and mechanical properties of concrete.

Residual compressive strength of concrete exposed to high temperatures is influenced by the following factors (Thielen, 1994):

- (1) water to cement ratio,
- (2) cement to aggregate ratio,
- (3) type of aggregate,
- (4) type of cement,
- (5) water content of concrete before exposing it to high temperatures and
- (6) fire process.

The stress-strain relationship characterises the stresses and deformation capacities of fire exposed concrete (Fig. 5). Test results include a small portion of creep which develops during the stressed period. In case of strain controlled tests with increasing strain, a decrease of stress is observed after the peak stress has been reached (CEB bulletin 208, 1991)

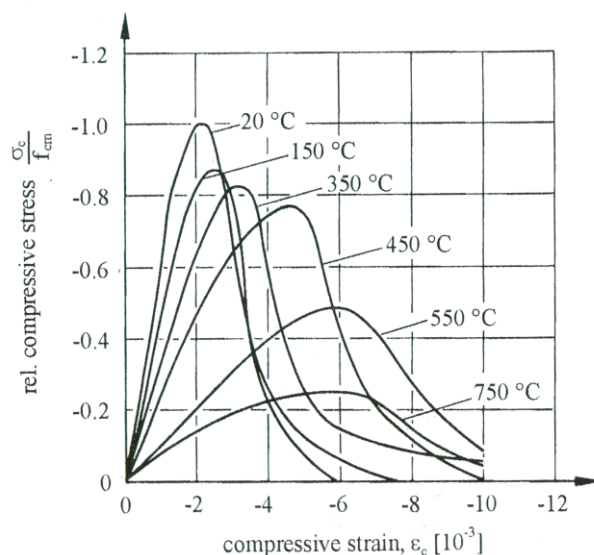


Fig. 5.

Stress-strain relationship for concrete with quartz gravel aggregate as a function of temperature (Schneider, Lebeda 2000)

Development of residual compressive strength after fire is demonstrated in Fig. 6. The following conclusions could we drawn:

- A strength valley is observed for relatively low values of maximal temperatures, i.e. a small strength decrease then small increase between 20°C to 300°C respectively. This valley might be explained by the pore water content of tested concretes at an age of 28 days. The valley ends up with about 100% strength. The valley could be explained by the relatively high pore water content of the 28 days concrete specimens.
- This valley is followed by decrease of compressive strength for higher values of maximal temperatures.
- Most considerable reduction of compressive strength took place between 400°C and 800°C.

The type of aggregate has a large influence on the reduction of compressive strengths of concrete (Fig. 6).

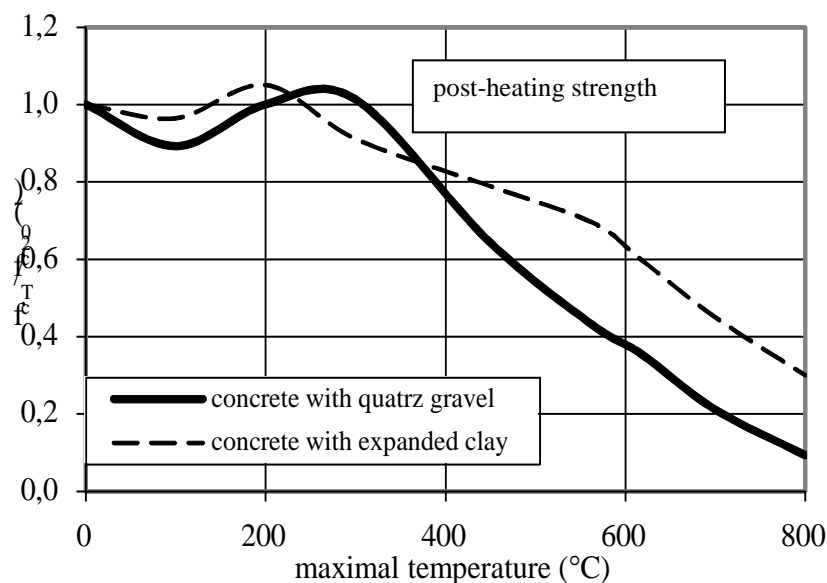


Fig. 6:

The residual compressive strength of concrete in function of temperature and of type of aggregate (Schneider, 1888)

Development of residual compressive strength during fire (i.e. in hot strength) is presented in Fig. 7. Comparison of Fig. 6 (post-heating strength) and Fig. 7 (hot strength) give the following conclusions (Schneider, Lebeda, 2000):

- hot strength reduction up to 300°C is most considerable and even a small increase was possible for 30% preloading (The strength valley doesn't appear).
- Increase of preloading up to 30% causes increase in residual hot strength.
- Hot strength values for high temperatures can be slightly higher than post-heating strength.

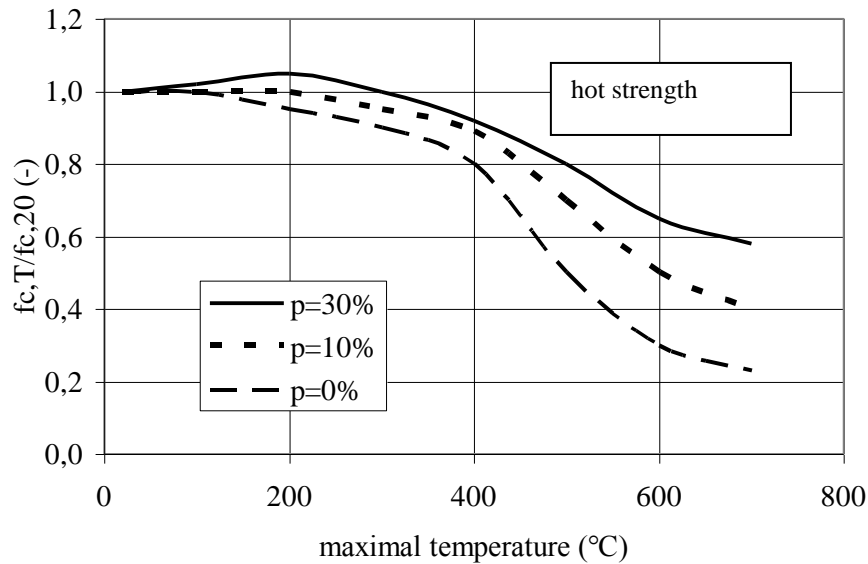


Fig. 7.
The residual compressive strength of concrete as functions of temperature and pre-loading (Schneider, 1988)

4. SPALLING OF CONCRETE COVER

Spalling of concrete cover may have two reasons: (1) internal vapour pressure (mainly for conventional concretes) and (2) overloading of concrete compressed zones (mainly for high strength concretes). The spalling mechanism of concrete cover can be seen in Fig. 8.

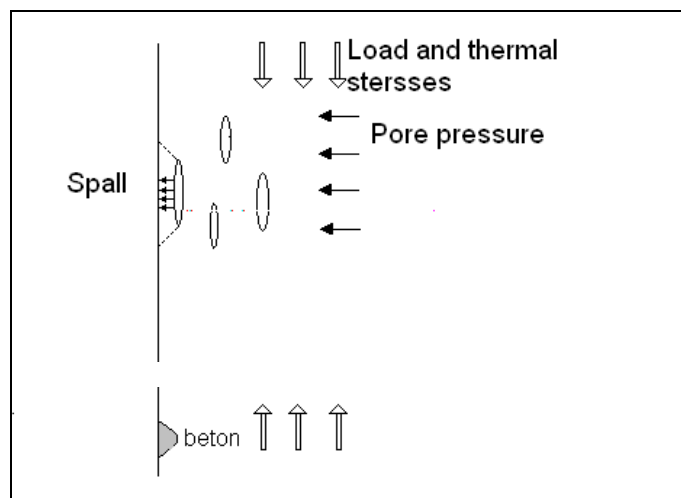
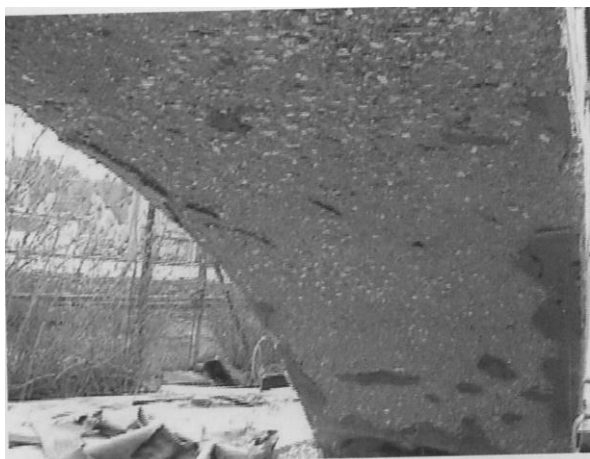


Fig. 8.
Mechanism of spalling (Høj, 2005)

Especially in tunnels it is important to avoid spalling of concrete cover. In Austria, in compliance with valid technical regulations, it is mandatory to use synthetic fibres for construction of tunnels.

A great number of experiments supported that the application of synthetic fibres considerably reduced the danger of spalling of concrete cover. Experiments with tunnel segments (length 11 m, height 2 m) carried out by Mörth, Haberland, Horvath and Mayer (2005) indicated, that the cover of the polypropylene fibre reinforced concrete did not spall *Fig. 9. a and b*).



a) without fibre reinforcement



b) with 2 kg/m³ polypropylene fibre reinforcement

Fig. 9:

*Tunnel segments after exposure to 1200°C temperature
(Mörth, Haberland, Horvath, Mayer, 2005)*

Fig. 10 shows that in case of polypropylene fibre reinforcement the possibility of spalling of concrete cover can be decreased. By increasing the fibre reinforcement spalling of concrete cover decreased.

Janson and Boström (2005) tested slender concrete columns of different concrete compositions. If concrete has been reinforced with polypropylene fibers independent of its composition the area of spalled concrete cover essentially decreased.



*with 1 kg/m³ polypropylene
fibre reinforcement*

*with 3 kg/m³ polypropylene fibre
reinforcement*

Produced without fibre reinforcement

Fig. 10.

Behaviour of tunnel segments produced with different fibre contents of polypropylene fibers, standard heating curve (<http://www.b-b-t.ch/produkte/kunststoff3.html>, BBT Trading & Consulting GmbH)

Fig. 11 a and b) Walter, Kari, Kusterle and Lindlbauer (2005) on reinforced concrete slabs with or without polymeric fibres. Two hours heating up to 1200°C produced similar results to the according to *Fig. 10*, i. e. considerably better behaviour with polymeric fibres.



a) without fibre reinforcement



b) with 2 kg/m³ synthetic fibre reinforcement

Fig. 11.

*Surface of the slabs after 2-hour fire exposure, standard heating curve
(Walter, Kari, Kusterle, Lindlbauer, 2005)*

Utilisation of synthetic fibres do not only reduce the probability of spalling of concrete cover layer, but also reduces the residual compressive strength.

A group of researchers (Horiguchi, 2005) experimentally proved on cylinders that the addition of synthetic or steel fibres has changed the value of the residual compressive strength.

5. CONCLUSIONS

Present paper summarizes the most important influences of fire on concrete. Concrete has excellent properties in regards of fire resistance compared with other materials and can be used to shield other structural materials such as steel. When exposed it to high temperature, concrete undergoes changes in its chemical composition, physical structure and water content. Such changes are reflected by changes in the physical and mechanical properties of concrete that are associated with temperature increase.

Deterioration of concrete at high temperatures has two forms: (1) local damage in the material itself (*Fig. 1*) and global damage resulting the failure of the elements (*Fig. 2*).

The residual compressive strength of concrete exposed to high temperatures is influenced by the following factors: (1) water to cement ratio, (2) cement to aggregate ratio, (3) type of aggregate, (4) type of cement, (5) water content of concrete before exposing it to high temperatures and (6) the fire process (Thielen, 1994).

We should distinguish between post-heating strength and hot strength of concrete. In both most considerable strength reduction takes place in both cases between 400°C and 800°C. Hot strength values for high temperatures can be slightly higher than post-heating strength.

Strength valley is observed for relatively low values of maximal temperatures, i.e. a small strength decrease then small increase between 20°C to 300°C, respectively.

Especially in tunnels it is important to avoid spalling of concrete cover. A great number of experiments supported that the application of synthetic fibres considerably reduced the danger of spalling of concrete cover.

An extensive experimental study is running at the Budapest University of Technology and Economics on temperature changes of concrete parameters like type of cement, type of aggregate and type of fibre.

6. REFERENCES

- In case of fire the behaviour of the expanded clay aggregate needs further experiments, but so far, it looks promising if synthetic fibres are also added. CEB Bulletin D'Information Number 208 (1991): „Fire design of concrete structures” fib bulletin 38, (2007): “Fire design of concrete structures- materials, structures and modelling”, ISBN: 978-2-88394-078-9
- Hinrichsmeyer, K. (1987): „Strukturorientierte Analyse und Modellbeschreibung der thermischen Schädigung von Beton”, Heft 74 IBMB, Braunschweig
- Horiguchi, T. (2005): „Combination of Synthetic and Steel Fibres Reinforcement for Fire Resistance of High Strength Concrete”, *Proceedings of Central European Congress on Concrete Engineering* 8.-9. Sept. 2005 Graz pp. 59-64.
- Janson, R., Boström, L. (2004): ”Experimental investigation on concrete spalling in fire.” *Proceedings for Fire Design of Concrete Structures: What now?, What next?* (Eds.: P. G. Gambarova, R. Felicieti, A. Meda, P. Riva) Milan, Dec. 2-3, 2004, pp.115-120.
- Khoury, G. A., Grainger, B. N., Sullivan, P. J. E. (1985): “Transient thermal strain of concrete: literature review, conditions within specimen and behaviour of individual constituents”, *Magazine of Concrete Research*, Vol. 37, No. 132, 1985 pp. 37-48.
- Kordina, K., Meyer-Ottens, C. (1981): „*Beton Brandschutz Handbuch.*“ 1. Auflage, Beton-Verlag GmbH, Düsseldorf
- Kordina, K. (1997): „Fire resistance of reinforced concrete beams“ (Über das Brandverhalten punktgeschützter Stahlbetonbalken), *Deutscher Ausschuss für Stahlbeton*, Heft 479, ISSN 0171-7197, Beuth Verlag GmbH, Berlin, 1997.
- Mörth, W., Haberland Ch., Horvath J., Mayer A.(2005): „Behaviour of Optimized Tunnel Concrete with Special Aggregates at High Temperature”, *Proceedings of Central European Congress on Concrete Engineering* 8.-9. Sept. 2005 Graz pp. 41-50
- Høj, N. P.(2005): „Keep concrete attractive - Fire design of concrete structures”, *Proceedings of fib symposium on Keep concrete attractive*, edited by Gy. L. Balázs, A. Borosnyói , 23-25 May 2005 Budapest, pp.1097-1105
- Thielen, K. Ch. (1994): „Strength and Deformation of Concrete Subjected to high Temperature and Biaxial Stress-Test and Modelling“ (Festigkeit und Verformung von Beton bei hoher Temperatur und biaxialer Beanspruchung - Versuche und Modellbildung), *Deutscher Ausschuss für Stahlbeton*, Heft 437 Beuth Verlag GmbH, Berlin
- Schneider, U., Lebeda, C. (2000): „*Baulicher Brandschutz*“, Stuttgart; Berlin; Köln: Kohlhammer, 2000
- Schneider, U. (1988): “Concrete at high temperatures-a general review”, *Fire Safety Journal*, Vol 13, 1988, pp. 55-68
- Schneider, U., Weiß, R. (1997): „Kinetische Betrachtungen über den thermischen Abbau zementgebundener Betone und dessen mechanische Auswirkungen”, *Cement and Concrete Research*, Vol 11, 1997, pp. 22-29
- Walter, R., Kari H., Kusterle W., Lindlbauer W. (2005): „Analysis of the Load-bearing Capacity of Fibre Reinforced Concrete During Fire”, *Proceedings of Central European Congress on Concrete Engineering* 8.-9. Sept. 2005, Graz pp. 54-59
- Waubke, N. V. (1997): „Physical analysis of strength reduction of concrete up to 1000 °C“ (Über einen physikalischen Gesichtspunkt der Festigkeitsverluste von Portlandzementbetonen bei Temperaturen bis 1000 °C-Brandverhalten von Bauteilen), Dissertation, TU Braunschweig, 1973.

http://upload.wikimedia.org/wikipedia/commons/9/93/Log_in_fireplace.jpg

<http://www.b-b-t.ch/produkte/kunststoff3.html>

<http://www.polizia.ti.ch>

Stability in Bending and Axial Compression of Steel Members

A nyomóerőre és hajlítónyomatékra igénybevett acél tartó stabilitása

Stabilitatea barei metalice solicitată la compresiune și încovoiere

Ștefan GUȚIU, Gavril KÖLLŐ, Petru MOGA, Cătălin MOGA

Railway Bridge Department at the Technical University of Cluj-Napoca, Romania,
Civil Engineering Faculty

ÖSSZEFOGLALÓ

Ebben a tanulmányban bemutatásra kerül az általános ellenőrzési módszer a nyomóerőre és hajlítónyomatékra igénybevett szimmetrikus keresztmetszetű tartó esetében az Eurocode 3 *Design of Steel Structures (EN 1993-1-1:2003: General rules and rules for buildings; EN 1993-1-5: 2004: Plated structural elements)* szerint. A bemutatott gyakorlati alkalmazás egy 12 m hosszú I tartóra vonatkozik amelyet hajlítónyomaték $M_{ed} = 500$ kNm és nyomóerő $N_{edy} = 1200$ kN valamint nyíróerő $V_{ed} = 400$ kN vesz igénybe.

A bemutatott gyakorlati alkalmazás segít megérteni az ellenőrzési módszert és az európai szabványok alkalmazását.

REZUMAT

În lucrare se prezintă metodologia de verificare la stabilitate generală (flambaj) a barei cu secțiune transversală dublu simetrică, solicitată la compresiune cu încovoiere, în conformitate cu Eurocode 3: *Design of Steel Structures (EN 1993-1-1:2003: General rules and rules for buildings; EN 1993-1-5: 2004: Plated structural elements)*.

Exemplul numeric privind verificarea la flambaj general a unui element cu secțiune dublu T simetrică, solicitat la compresiune și încovoiere, prezentat detaliat în lucrare, permite înțelegerea metodologiei de aplicare a euronormeii în vederea implementării acesteia în activitatea de proiectare.

ABSTRACT

This paper presents the stability verification methodology of uniform members with double symmetric cross section subjected to bending and axial compression in accordance with Eurocode 3: *Design of Steel Structures (EN 1993-1-1:2003: General rules and rules for buildings; EN 1993-1-5: 2004: Plated structural elements)*.

The numerical example also detailed in the paper, concerning the buckling verification of a member with a double T symmetric cross section, subjected to monoaxial bending and axial compression is useful to understand the design methodology.

1. INTRODUCTION

The general stability of a steel member subjected to bending and compression is a complex phenomenon where the flexural and torsional buckling, the lateral buckling of the compression flange and their interaction have been taken into account. The cross sections are divided into four cross section classes with the role of identifying the extend to which the resistance and rotation capacity of the cross section is limited by its local buckling resistance. In Class 4 cross sections effective width may be used to make the necessary allowances for reduction in resistance due to the effects of local buckling. For a Class 4 cross section it should also

be determined the possible shift e_N of the centroid of the effective area A_{eff} relative to the centre of gravity of the gross cross section and the resulting additional moment: $\Delta M_{Ed} = N_{Ed} \cdot e_N$

2. UNIFORM MEMBERS IN BENDING AND AXIAL COMPRESSION

In accordance with [1], unless second order analysis is carried out, the stability of uniform members with double symmetric cross sections which are subjected to combined bending and compression should satisfy:

$$\chi_y \frac{N_{Ed}}{\gamma_{M1} \frac{N_{Rk}}{\gamma_{M1}}} + k_{yy} \frac{M_{y.Ed} + \Delta M_{y.Ed}}{\chi_{LT} \frac{M_{y.Rk}}{\gamma_{M1}}} + k_{yz} \frac{M_{z.Ed} + \Delta M_{z.Ed}}{\gamma_{M1}} \leq 1 \quad (1.a)$$

$$\chi_z \frac{N_{Ed}}{\gamma_{M1} \frac{N_{Rk}}{\gamma_{M1}}} + k_{zy} \frac{M_{y.Ed} + \Delta M_{y.Ed}}{\chi_{LT} \frac{M_{y.Rk}}{\gamma_{M1}}} + k_{zz} \frac{M_{z.Ed} + \Delta M_{z.Ed}}{\gamma_{M1}} \leq 1 \quad (1.b)$$

where: $N_{Ed}, M_{y.Ed}, M_{z.Ed}$ – the design values of the compression force and the maximum moments about the y-y and z-z axis; $\Delta M_{y.Ed}, \Delta M_{z.Ed}$ – the moments due to the shift of the centroidal axis for class 4 sections; χ_y, χ_z – the reduction factors due to flexural buckling; χ_{LT} – the reduction factor due to lateral torsional buckling; $k_{yy}, k_{yz}, k_{zy}, k_{zz}$ – the interaction factors which may be obtained from Annex A (alternative method 1) or from Annex B 9 Alternative method 2).

The characteristic resistances $N_{Rk} = A_i \cdot f_y$; $M_{Rk} = W \cdot f_y$ and $\Delta M_{Ed} = e_N \cdot N_{Ed}$ will be evaluated in accordance with Table 1.

Table 1

CLASA	1	2	3	4
A_i	A	A	A	A_{eff}
W_y	$W_{pl,y}$	$W_{pl,y}$	$W_{el,y}$	$W_{eff,y}$
W_z	$W_{pl,z}$	$W_{pl,z}$	$W_{el,z}$	$W_{eff,z}$
$\Delta M_{y.Ed}$	0	0	0	$e_{N,y} \cdot N_{Ed}$
$\Delta M_{z.Ed}$	0	0	0	$e_{N,z} \cdot N_{Ed}$

The reduction factor χ_{TF} is determined function of the torsional – flexural non-dimensional slenderness, $\bar{\lambda}_{TF}$:

$$\bar{\lambda}_{TF} = \sqrt{\frac{A_i f_y}{N_{cr}}}; \text{ where: } A_i = \begin{cases} A & \text{sections Class 1; 2; 3} \\ A_{eff} & \text{section Class 4} \end{cases} \quad (2)$$

$$N_{cr} = \min \left\{ \begin{aligned} N_{cr.T} &= \frac{A_g}{I_0} \left(GI_t + \frac{\pi^2 EI_w}{L_{cr.T}^2} \right) \\ N_{cr.TF} &= \frac{I_0}{2(I_y + I_z)} \left[(N_{cr.z} + N_{cr.T}) - \sqrt{(N_{cr.z} + N_{cr.T})^2 - 4 \frac{(I_y + I_z)}{I_0} N_{cr.z} N_{cr.T}} \right] \end{aligned} \right. \quad (3)$$

3. WORKING EXAMPLE

The general stability in accordance with EN 1993-1-1:2003 of a uniform member with a double symmetric cross section subjected to bending and axial compression is checked. The following design data are given:

Member cross section

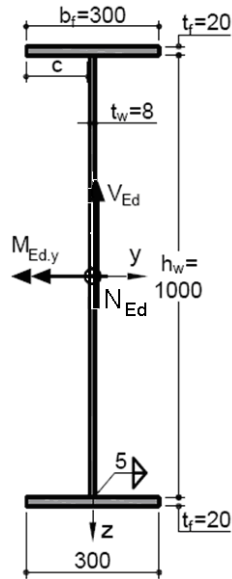


Fig. 1.

Steel S355 ($f_y = 355 \text{ N/mm}^2$; $\varepsilon = 0.81$)

Loadings:

- $N_{Ed} = 1200 \text{ kN}$
- $M_{Ed,y} = 500 \text{ kN} \cdot \text{m}$ (constant pe L)
- $V_{Ed} = 400 \text{ kN}$

Lengths:

- $L = 12.0 \text{ m}$
- $l_{fy} = L_{cr,y} = 12.0 \text{ m}$
- $l_{fz} = L_{cr,z} = L_{cr,LT} = 4.0 \text{ m}$

3.1. Cross section characteristics

Gross section:

- $A = 200 \text{ cm}^2$
- $I_y = 378\,817 \text{ cm}^4$
- $W_{el,y} = 7\,285 \text{ cm}^3$
- $W_{pl,y} = 8\,120 \text{ cm}^3$
- $I_z = 9\,004 \text{ cm}^4$
- $W_{el,z} = 600.3 \text{ cm}^3$
- $W_{pl,z} = 916 \text{ cm}^3$
- $I_{\omega}(I_w) = 2.341 \cdot 10^7 \text{ cm}^6$

Cross section Class

Compression flange

The flange is an outstand element under uniform compression ($\psi = 1$; $k_{\sigma} = 0.43$).

$$\frac{c}{t_f} = \frac{[b_f - (t_w + 2\sqrt{2} \cdot a_w)]/2}{t_f} = \frac{[300 - (8 + 2\sqrt{2} \cdot 5)]/2}{20} = 6.95 < 9 \cdot \varepsilon = 7.29 \Rightarrow$$

The flange is Class 1.

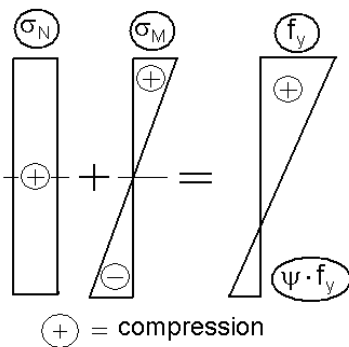


Fig. 2.

Web

The web is subjected to bending and compression. The stress ratio at ULS is given by (Figure 2):

$$\psi = \frac{2 N_{Ed}}{A f_y} - 1 = \frac{2 \cdot 1200 \cdot 10^2}{200 \cdot 3550} - 1 = -0.66 > -1$$

$$\frac{c}{t_w} = 123.2 > \frac{42 \cdot \varepsilon}{0.67 + 0.33\psi} = 75.2 \Rightarrow \text{The web is Class 4}$$

The section is Class 4 \Rightarrow The verification of the member will be based on the elastic resistance of the effective cross-section. **Effective cross section**

Effective area

The effective area of the cross section is determined under compression only - EN 1993-1-1. § 6.2.9.3(2).

Flange

The flange is Class 1 $\Rightarrow A_{f,eff} = A_f$

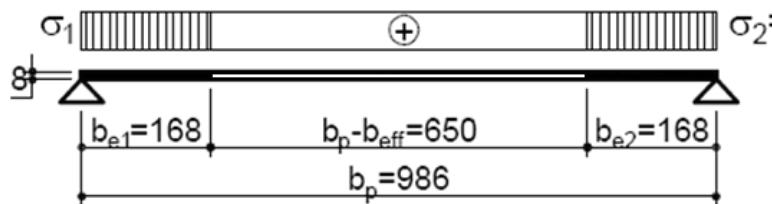
Web

The web is an internal element subjected to uniform compression, $\psi = 1$; $k\sigma = 4$, Figure 3.

$$\frac{c}{t_w} = \frac{h_w - 2\sqrt{2} \cdot a_w}{t_w} = \frac{1000 - 2\sqrt{2} \cdot 5}{8} = 123.2 > 42\varepsilon = 34 \Rightarrow \text{Class 4}$$

Slenderness: $\bar{\lambda}_p = \frac{c/t_w}{28.4 \cdot \varepsilon \cdot \sqrt{k\sigma}} = \frac{986/8}{28.4 \cdot 0.81 \cdot \sqrt{4}} = 2.68 > 0.673$

Reduction factor: $\rho = \frac{\bar{\lambda}_p - 0.055(3 + \psi)}{\bar{\lambda}_p^2} = \frac{2.68 - 0.055(3 + 1)}{2.68^2} = 0.34 < 1$



Effective width:
 $b_{eff} = \rho \cdot c = 0.34 \cdot 986 = 336 \text{ mm}$
 $b_{e1} = b_{e2} = 0.5 \cdot b_{eff} = 168 \text{ mm}$

⊕ – compression

Fig. 3.

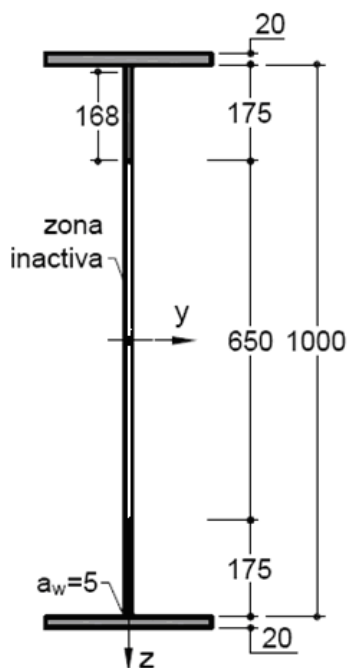


Fig. 4.

Figure 4 presents the effective section taking into account the compression only.

It is obtained:

$$A_{eff} = 200 - 0.8 \cdot 65 = 148 \text{ cm}^2$$

Effective elastic modulus

The effective elastic modulus is determined under bending only - EN 1993-1-1. § 6.2.9.3(2).

Flange

The flange is Class 1 $\Rightarrow A_{f,eff} = A_f$

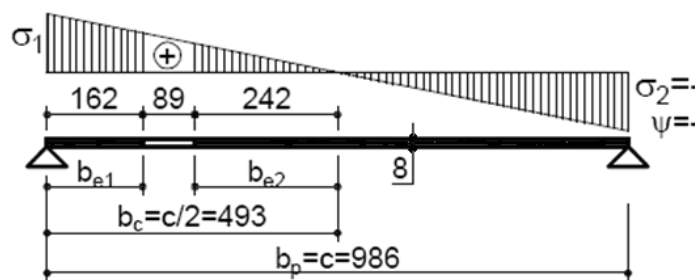
Web

The web is an internal element subjected to bending, $\psi = -1$; $k\sigma = 23.9$, Figure 5.

$$\frac{c}{t_w} = 123.2 > 124\varepsilon = 100.44 \Rightarrow \text{Class 4}$$

$$\text{Slenderness: } \bar{\lambda}_p = \frac{c/t_w}{28.4 \cdot \varepsilon \cdot \sqrt{k\sigma}} = \frac{986/8}{28.4 \cdot 0.81 \cdot \sqrt{23.9}} = 1.1 > 0.673$$

$$\text{Reduction factor: } \rho = \frac{\bar{\lambda}_p - 0.055(3 + \psi)}{\bar{\lambda}_p^2} = \frac{1.1 - 0.055(3 - 1)}{1.1^2} = 0.82 < 1$$



Effective width:

$$b_{eff} = \rho \cdot b_c = 0.82 \cdot 493 = 404 \text{ mm}$$

$$b_{e1} = 0.4 \cdot b_{eff} = 162 \text{ mm}$$

$$b_{e2} = 0.6 \cdot b_{eff} = 242 \text{ mm}$$

Fig. 5.

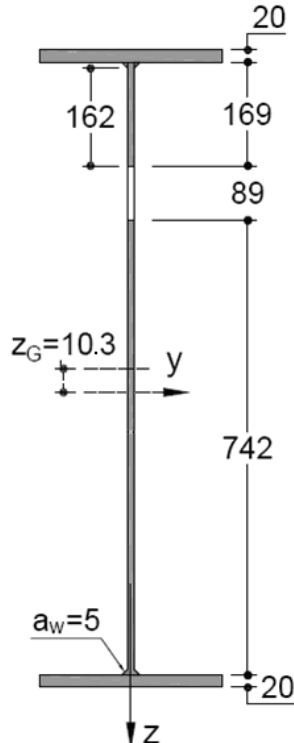


Fig. 6.

Figure 6 presents the effective section taking into account the bending only.

It is obtained:

$$I_{eff.y} = 3.66 \cdot 10^5 \text{ cm}^4$$

$$W_{eff.y} = 6973 \text{ cm}^3$$

3.2. Verification of the buckling resistance

In this case we have:

$e_{Ny} = e_{Nz} = 0 \Rightarrow \Delta M_{y,Rd} = \Delta M_{z,Rd} = 0$; $M_{z,Ed} = 0$ The relations (1.a,b) become:

$$\frac{N_{Ed}}{\chi_y \frac{N_{Rk}}{\gamma_{M1}}} + k_{yy} \frac{M_{y,Ed}}{\chi_{LT} \frac{M_{y,Rk}}{\gamma_{M1}}} \leq 1$$

$$\frac{N_{Ed}}{\chi_z \frac{N_{Rk}}{\gamma_{M1}}} + k_{zy} \frac{M_{y,Ed}}{\chi_{LT} \frac{M_{y,Rk}}{\gamma_{M1}}} \leq 1$$

The k_{yy} and k_{zy} factors will be calculated using the Annex A of EN 1993-1-1.

Buckling about y-y - axis

$$N_{cr,y} = \pi^2 \frac{EI_y}{L_{cr,y}^2} = \pi^2 \frac{2.1 \cdot 10^6 \cdot 3.788 \cdot 10^5}{1200^2} \cdot 10^{-2} = 5.45 \cdot 10^4 \text{ kN}$$

$$\bar{\lambda}_y = \sqrt{\frac{A_{eff} f_y}{N_{cr,y}}} = \sqrt{\frac{148 \cdot 3550}{5.45 \cdot 10^6}} = 0.31 \Rightarrow \chi_y = 0.96 \quad (\text{curve „b”} \quad t_f < 40)$$

It is obtained:

$$N_{b,y,Rd} = \chi_y \frac{N_{Rk}}{\gamma_{M1}} = \chi_y \frac{A_{eff} f_y}{\gamma_{M1}} = 0.96 \frac{148 \cdot 3550}{1.1} \cdot 10^{-2} = 4\,585 \text{ kN}$$

Buckling about z-z - axis

$$N_{cr,z} = \pi^2 \frac{EI_z}{L_{cr,z}^2} = \pi^2 \frac{2.1 \cdot 10^6 \cdot 9\,004}{400^2} \cdot 10^{-2} = 1.166 \cdot 10^4 \text{ kN}$$

$$\bar{\lambda}_z = \sqrt{\frac{A_{eff} f_y}{N_{cr,z}}} = \sqrt{\frac{148 \cdot 3550}{1.166 \cdot 10^6}} = 0.67 \Rightarrow \chi_z = 0.74 \quad (\text{curve „c”})$$

It is obtained:

$$N_{b,z,Rd} = \chi_z \frac{N_{Rk}}{\gamma_{M1}} = \chi_z \frac{A_{eff} f_y}{\gamma_{M1}} = 0.74 \frac{148 \cdot 3550}{1.1} \cdot 10^{-2} = 3\,535 \text{ kN}$$

Lateral torsional buckling

The critical moment for a doubly symmetrical section ($L_{cr,LT} = 4.0 \text{ m}$):

$$M_{cr} = C_1 \frac{\pi^2 EI_z}{L_{cr,LT}^2} \sqrt{I_w + \frac{L_{cr,LT}^2 GI_t}{\pi^2 EI_z}}$$

$$= 1 \cdot \frac{\pi^2 \cdot 2.1 \cdot 10^6 \cdot 9\,004}{400^2} \sqrt{\frac{2.341 \cdot 10^7}{9\,004} + \frac{400^2 \cdot 0.807 \cdot 10^6 \cdot 177}{\pi^2 \cdot 2.1 \cdot 10^6 \cdot 9\,004}} \cdot 10^{-4} = 6079 \text{ kNm}$$

where: $C_1 = 1$ - for M constant ($\psi = +1$)

The slenderness for lateral torsional buckling:

$$\bar{\lambda}_{LT} = \sqrt{\frac{W_{eff,y} f_y}{M_{cr}}} = \sqrt{\frac{6973 \cdot 3550}{6079 \cdot 10^4}} = 0.62 \Rightarrow \chi_{LT} = 0.69 \quad (\text{curve „d”} - \alpha_{LT} = 0.76)$$

It is obtained:

$$M_{b,Rd} = \chi_{LT} \frac{M_{y,Rk}}{\gamma_{M1}} = \chi_{LT} \frac{W_{eff,y} f_y}{\gamma_{M1}} = 0.69 \frac{6973 \cdot 3550}{1.1} \cdot 10^{-4} = 1553 \text{ kNm}$$

Factors μ_{yy} and μ_{zy} (Annex A – EN 1993-1-1)

$$k_{yy} = C_{my} C_{m.LT} \frac{\mu_y}{1 - \frac{N_{Ed}}{N_{cr.y}}} = 1.022 \cdot C_{my} C_{m.LT}$$

$$k_{zy} = C_{my} C_{m.LT} \frac{\mu_z}{1 - \frac{N_{Ed}}{N_{cr.y}}} = 1 \cdot C_{my} C_{m.LT}$$

where:

$$\mu_y = \frac{1 - \frac{N_{Ed}}{N_{cr.y}}}{1 - \chi_y \frac{N_{Ed}}{N_{cr.y}}} = \frac{1 - \frac{1200}{5.45 \cdot 10^4}}{1 - 0.97 \frac{1200}{5.45 \cdot 10^4}} = 1$$

$$\mu_z = \frac{1 - \frac{N_{Ed}}{N_{cr.z}}}{1 - \chi_z \frac{N_{Ed}}{N_{cr.z}}} = \frac{1 - \frac{1200}{1.166 \cdot 10^4}}{1 - 0.80 \frac{1200}{1.166 \cdot 10^4}} = 0.98$$

It is checked the relation which defines the susceptibility to torsional deformations:

$$\begin{aligned} \bar{\lambda}_0 &\leq \bar{\lambda}_{0.lim} = 0.2 \sqrt{C_1} \sqrt[4]{\left(1 - \frac{N_{Ed}}{N_{cr.z}}\right) \left(1 - \frac{N_{Ed}}{N_{cr.TF}}\right)} = \\ &= 0.2 \sqrt{1} \sqrt[4]{\left(1 - \frac{1200}{1.166 \cdot 10^4}\right) \left(1 - \frac{1200}{1.64 \cdot 10^4}\right)} = 0.19 \end{aligned}$$

where: $\bar{\lambda}_0 = \lambda_{LT} = 0.62$ - the slenderness for lateral torsional buckling for an uniform moment.

For a doubly symmetrical section $N_{cr.TF} = N_{cr.T}$:

$$\begin{aligned} N_{cr.TF} = N_{cr.T} &= \frac{A}{I_0} \left(GI_t + \frac{\pi^2 EI_w}{L_{LT}^2} \right) = \\ &= \frac{200}{3.87 \cdot 10^5} \left(0.807 \cdot 10^6 \cdot 177 + \frac{\pi^2 2.1 \cdot 10^6 \cdot 2.341 \cdot 10^7}{400^2} \right) = 1.64 \cdot 10^6 \text{ daN} \end{aligned}$$

$$I_0 = I_y + I_z = 3.878 \cdot 10^5 \text{ cm}^4; \quad I_t = \frac{1}{3} (2 \cdot 30 \cdot 2^3 + 100 \cdot 0.8^3) = 177 \text{ cm}^4$$

For $\bar{\lambda}_0 = 0.62 > \bar{\lambda}_{0.lim} = 0.19$:

$$C_{my} = C_{my.0} + (1 - C_{my.0}) \frac{\sqrt{\varepsilon_y} a_{LT}}{1 + \sqrt{\varepsilon_y} a_{LT}} = 1$$

where:

$$\varepsilon_y = \frac{M_{y.Ed}}{N_{Ed}} \frac{A_{eff}}{W_{eff.y}} = \frac{500 \cdot 10^4}{1200 \cdot 10^2} \frac{148}{7031} = 0.88$$

$$a_{LT} = 1 - \frac{I_t}{I_y} \approx 1$$

For $\psi_y = 1$ (uniform moment), the equivalent uniform moment factor is:

$$C_{my.0} = 0.79 + 0.21 \cdot \psi_y + 0.36 (\psi_y - 0.33) \frac{N_{Ed}}{N_{cr.y}} = 1$$

Factor $C_{m.LT}$:

$$C_{m.LT} = C_{my}^2 \frac{a_{LT}}{\sqrt{\left(1 - \frac{N_{Ed}}{N_{cr.z}}\right) \left(1 - \frac{N_{Ed}}{N_{cr.T}}\right)}} = 1^2 \frac{1}{\sqrt{\left(1 - \frac{1200}{1.166 \cdot 10^4}\right) \left(1 - \frac{1200}{1.64 \cdot 10^4}\right)}} = 1.09 > 1$$

It is obtained:

$$k_{yy} = 1.11; \quad k_{zy} = 1.09$$

The interaction formulae for the member buckling which is subjected to bending and compression are:

$$\frac{N_{Ed}}{\chi_y \frac{N_{Rk}}{\gamma_{M1}}} + k_{yy} \frac{M_{y,Ed}}{\chi_{LT} \frac{M_{y,Rk}}{\gamma_{M1}}} = \frac{1200}{4585} + 1.11 \frac{500}{1553} = 0.62 < 1$$

$$\frac{N_{Ed}}{\chi_z \frac{N_{Rk}}{\gamma_{M1}}} + k_{zy} \frac{M_{y,Ed}}{\chi_{LT} \frac{M_{y,Rk}}{\gamma_{M1}}} = \frac{1200}{3535} + 1.09 \frac{500}{1553} = 0.69 < 1$$

4. FINAL REMARKS

The general stability of the steel member subjected to bending and axial compression in accordance with EN 1993-1-1 takes into account the following aspects:

- the flexural buckling by using the reduction factors χ_y and χ_z ;
- the lateral torsional buckling by using the reduction factor χ_{LT} ;
- the effective properties of the cross section;
- the moments due to the shift of the centroidal axis for class 4 sections;
- the interaction between different loadings by using the interaction factors $k_{yy}, k_{yz}, k_{zy}, k_{zz}$

REFERENCES

- [1.] *** Eurocode 3: Design of steel structures. EN 1993-1-1:2003: General rules and rules for buildings
- [2.] *** Eurocode 3: Design of steel structures EN 1993-1-5: 2004: Plated structural elements
- [3.] *** SR EN 1993-1-1: 2006. Eurocod 3: Proiectarea structurilor de oțel. Partea 1-1: Reguli generale și reguli pentru clădiri
- [4.] *** ACCESS STEEL. NCCI: Mono-symmetrical uniform members under bending and axial compression. SNO30a-EN-EU. 2006
- [5.] *** Moga,P.,Păcurar,V.,Guțiu,Șt.,Moga,C.: Calculul elementelor metalice. Norme române-Eurocode 3. U.T.PRESS. 2006
- [6.] *** Moga,P.,Păcurar,V.,Guțiu,Șt.,Moga,C.: Construcții și poduri metalice. Aplicare euronorme. U.T.PRESS. 2007

Thin-Walled Composite Columns

Együttműködő öszvérkeresztmetszetű oszlopok megvalósítása vékony lemezek segítségével

Stâlpi cu secțiune compusă din bare cu pereți subțiri

Petru MOGA, Gavril KÖLLŐ, Ștefan GUȚIU, Cătălin MOGA

Railway Bridge Department at the Technical University of Cluj-Napoca, Romania,
Civil Engineering Faculty

ÖSSZEFOGLALÓ

A vékony keresztmetszetű lemezeket (BPS) amelyeket a lemezek hidegen való hajlításával hoztak létre.

Jól lehet használni az együttműködő öszvér keresztmetszetek létrehozásánál.

Ezek a keresztmetszetek használhatók tartógerendák, oszlopok, szélrácsok megvalósításánál.

Egyik fontos előnye a vékonyfalú (BPS) acéltartóból és betonból kialakított keresztmetszetű tartóknak, hogy így lehetséges egy széles skálán mozgó több típusú keresztmetszet kialakítása.

Az egyik hátránya az ilyen típusú tartóknak az, hogy a lemezek külső felületét biztosítani kell korózió ellen.

A jelen tanulmányban bemutatásra kerül néhány öszvér keresztmetszetű oszlop amelyet vékony keresztmetszetű lemezekkel valósítottak meg.

Összehasonlító elemzést mutatunk be a különböző típusú oszlopok teherbírását illetően.

REZUMAT

Barele cu pereți – BPS, realizate prin deformarea la rece a tablelor cu o grosime relativ redusă sunt utilizate atât ca secțiuni unitare, cât și sub formă de secțiuni compuse din unul sau mai multe profile, pentru cvasi totalitatea elementelor structurale – stâlpi, grinzi, contravântuiri, elemente de solidarizare etc.

Principalul avantaj oferit de BPS constă în faptul că se poate realiza o gamă foarte variată de tipuri de secțiuni transversale, din punct de vedere a formei și a dimensiunilor acestora, evitându-se asamblarea cu un număr mare de suduri longitudinale a tablelor.

Dezavantajul acestora constă în susceptibilitatea mai ridicată la fenomenul de coroziune exterioară, datorat grosimii reduse a tablelor, dar mai ales necesitatea de a menține în limite de siguranță a fenomenelor de instabilitate locală și generală.

În lucrare se propun pentru utilizare câteva tipuri de stâlpi cu secțiune compusă realizați din BPS și se prezintă o analiză comparativă privind capacitatea portantă la compresiune centrică a unor stâlpi din BPS realizați în diferite soluții constructive.

INTRODUCTION

The thin-walled are used for a large variety of structural members such as columns, girders, trusses etc, the main advantage of these consisting in various cross-section shapes which can be easily adapted to the external loading.

The disadvantages of these elements are a greater susceptibility to the corrosion phenomenon and to local and general buckling and stability.

This paper presents types of thin-walled cross-sections which can be used as concrete-filled tubular steel sections for composite columns and a comparative study concerning the load bearing capacity of the four cross-section types subjected to axial compression.

CONCRETE-FILLED THIN WALLED SECTIONS

THIN-WALLED CROSS-SECTIONS

Four types of concrete-filled thin-walled sections are proposed as composite steel-concrete column, as follows (Figure 1):

- Concrete-filled four thin-walled lipped angles with equal flanges (Fig. 1.a);
- Concrete-filled four thin-walled lipped angles with unequal flanges (Fig. 1.b);
- Concrete-filled two thin-walled lipped channels (Fig. 1.c);
- Concrete-filled two Σ shape sections (Fig. 1.d);

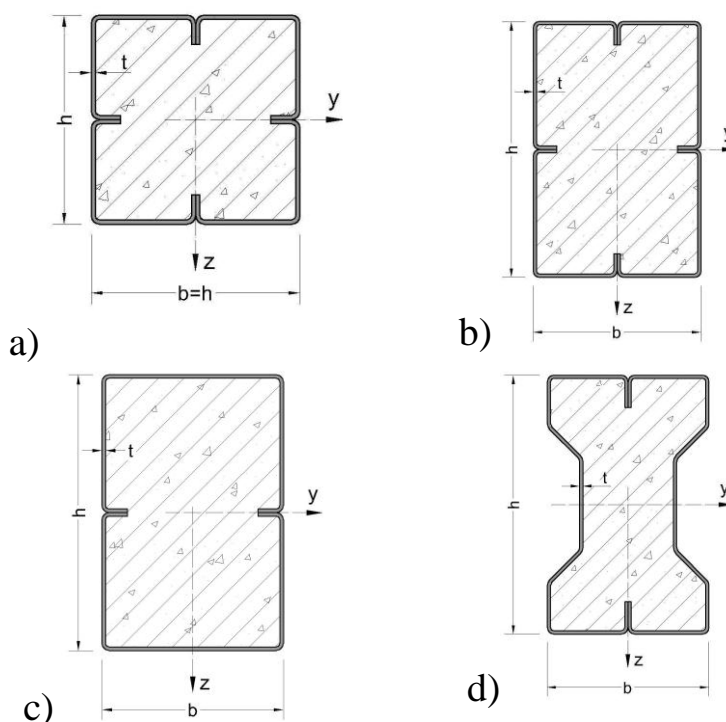


Fig. 1.

CROSS-SECTION CHARACTERISTICS

In accordance with EC 4 (EN 1994-1-1:2004), respectively with the Romanian standard SR EN 1994-1-1:2004 it is underlined that the local buckling of the steel section component can be neglected if the following conditions are fulfilled:

- concrete-filled rectangular steel section:

$$\max(h/t) = 52 \sqrt{\frac{235}{f_y}} \quad (1.a)$$

- concrete-filled circular steel section:

$$\max(d/t) = 90 \frac{235}{f_y} \quad (1.b)$$

If the steel wall plates slenderness is higher, the local buckling phenomenon has to be taken into account.

In accordance with EC 3. Part 1.5: *Plated structural elements* the characteristics of the effective cross-section are based on the effective width of the compression elements.

The effective width of the compression element should be obtained using the reduction factor for the plate buckling ρ .

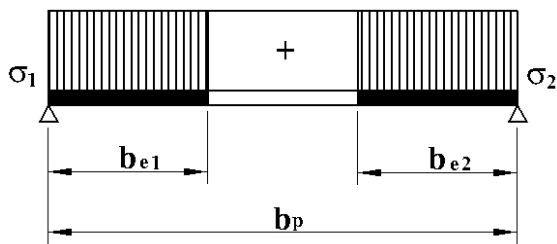
For internal axial compression elements, Figure 2 ($\sigma_1 = \sigma_2 \Rightarrow \Psi = 1$) the reduction factor ρ is given by:

$$\rho = \begin{cases} 1 & \text{for: } \bar{\lambda}_p \leq 0.673 \\ \frac{\bar{\lambda}_p - 0.22}{\bar{\lambda}_p^2} & \text{for: } \bar{\lambda}_p > 0.673 \end{cases} \quad (2)$$

$$\text{where: } \bar{\lambda}_p = \sqrt{\frac{f_y}{\sigma_{cr}}} = \frac{b_p/t}{28,4 \cdot \varepsilon \cdot \sqrt{k_\sigma}}; \quad \varepsilon = \sqrt{\frac{235}{f_y}}$$

$k_\sigma = 4$ – the buckling factor

b_p - the appropriate width of the plate.



$$\begin{aligned} \Psi &= +1: \\ b_{eff} &= \rho \cdot b_p \\ b_{e1} &= 0,5 \cdot b_{eff} \\ b_{e2} &= 0,5 \cdot b_{eff} \end{aligned}$$

Fig. 2.

Figure 3 presents the effective cross-section and the buckled shape of a composite column section.

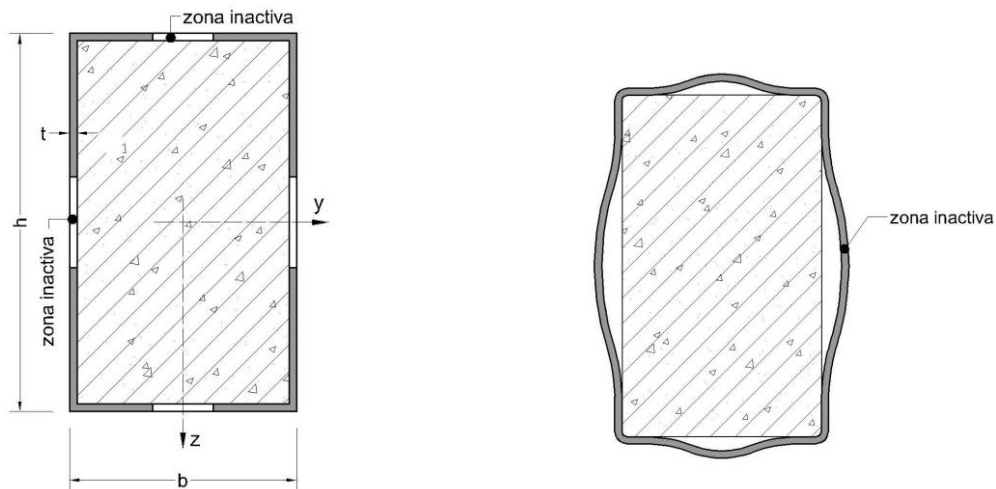


Fig. 3.

To avoid ineffective area of the steel component the steel cross-section has to be less than Class 4 and the following condition has to be fulfilled:

$$\bar{\lambda}_p \leq 0.673 \Rightarrow \rho = 1 \quad (3)$$

For axial compression ($k_\sigma = 4$) it results the limiting slenderness value of the steel wall panel:

$$\frac{b_p}{t} \leq 38.2 \cdot \varepsilon; \quad b_p = b - 3t \quad (4)$$

AXIAL COMPRESSION COMPOSITE COLUMN RESISTANCE

In accordance with Eurocode 4, the resistance capacity of an axial compression composite steel-concrete column is given by the expression:

$$N_{Rd} = \chi \cdot N_{pl,Rd} \quad (5)$$

For concrete-filled rectangular hollow section of Class 4, the plastic resistance to compression, $N_{pl,Rd}$, should be evaluated with the relation:

$$N_{pl,Rd} = A_{a,eff} \frac{f_y}{\gamma_a} + A_c \frac{f_{ck}}{\gamma_c} + A_s \frac{f_{sk}}{\gamma_s} \quad (6)$$

where:

- A_a ; A_c ; A_s – cross-section areas of steel, concrete and reinforcement;
- f_y ; f_{ck} ; f_{sk} – characteristic strengths of steel, concrete and reinforcement;
- γ_a ; γ_c ; γ_s – partial safety factors of steel, concrete and reinforcement;

The reduction factor for the relevant buckling mode, χ , is in term of the relevant relative slenderness $\bar{\lambda}$ and the relevant buckling curve for cross-section.

The effective elastic flexural stiffness of the composite column will be evaluated with the relation:

$$(EI)_{e,eff} = E_a I_{a,eff} + 0.6 E_{cm} I_c + E_s I_s \quad (7)$$

where:

- $I_{a,eff}$; I_c ; I_s – second moment of area of the structural steel effective section, the un-cracked concrete section and the reinforcement;
- E_a ; E_s – modulus of elasticity of structural steel and reinforcement;
- E_{cm} – secant modulus of elasticity of concrete.

The relevant relative slenderness is given by:

$$\bar{\lambda} = \sqrt{\frac{N_{pl,Rk}}{N_{cr}}} \quad (8)$$

where:

$$N_{pl,Rk} = A_{a,eff} f_y + A_c f_{ck} + A_s f_{sk} \quad (9)$$

$$N_{cr} = \frac{\pi^2 (EI)_{e,eff}}{l^2} \quad (10)$$

For members with high relative slenderness ratio (see EC 4), account should be taken to the influence of long-term effects on the effective elastic flexural stiffness.

The modulus E_{cm} will be reduced to E_c , evaluated with the relation:

$$E_c = E_{cm} \frac{1}{1 + (N_{G,Ed} / N_{Ed}) \varphi_t} \quad (11)$$

where:

- $N_{G,Ed}$ - part of the total design normal force N_{Ed} that is permanent;
- φ_t – creep coefficient according to EC 2.

3. COMPARATIVE ANALYSIS

The load carrying capacity (design resistance) of an axial compression column is evaluated. The column cross-section is built-up in the following solutions:

- Type A: Concrete-filled two longitudinally welded Σ shape steel section;
- Type B: Two longitudinally welded Σ shape hollow steel section (type A without filled-concrete);
- Type C: Concrete-filled a rectangular hollow steel section built-up by two lipped channels longitudinally welded;
- Type D: Rectangular hollow steel section built-up by two lipped channels longitudinally welded (type C without filled-concrete).

All of these four section types have the same main dimensions of the cross-section: $h=400$ mm and $b=250$ mm and have the same or close area of the steel component (respectively $A_g=77$ cm²), so the steel consumption is identically.

The calculation will be made relative to the main axis $y-y$ for a design column length (buckling length) $L=8.00$ m.

Design data

Materials:

Steel: S 235

$f_y = 235$ N/mm²

$E = 210000$ N/mm²

Concrete: C 20 / 25

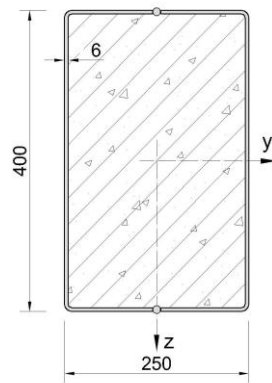
$f_{ck} = 20$ N/mm²

$E_{cm} = 29000$ N/mm²

Cross-sections and main design characteristics:

SECTION TYPE	MAIN DIMENSIONS	DESIGN CHARACTERISTICS	
A		$I_a = 17\,624$ cm ⁴ $A_a = 77$ cm ²	$I_c = 109\,442$ cm ⁴ $A_c = 733$ cm ²
B		$I_y = 17\,624$ cm ⁴ $A_g = A_{eff} = 77$ cm ²	

C



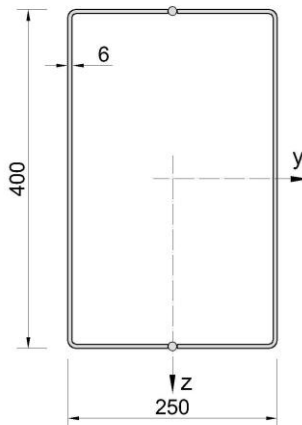
$$I_a = 17\,485 \text{ cm}^4$$

$$A_a = 76.5 \text{ cm}^2$$

$$I_c = 115\,848 \text{ cm}^4$$

$$A_c = 804 \text{ cm}^2$$

D



$$I_y = 17\,485 \text{ cm}^4$$

$$A_g = 76.5 \text{ cm}^2; A_{\text{eff}} = 63.66 \text{ cm}^2$$

Design resistance

Type A:

According to EC 3:

The largest wall panel has the slenderness:

$$\frac{c}{t} = \frac{140}{5} = 28 < 33 \cdot \varepsilon = 33 \Rightarrow \text{Class 1}$$

To evaluate the composite column design resistance, the cross-section being of Class 1, the characteristics of the gross section will be used.

According to EC 4:

$$N_{\text{pl.Rd}} = A_a \frac{f_y}{\gamma_a} + A_c \frac{f_{\text{ck}}}{\gamma_c} = 77 \frac{2350}{1.1} + 733 \frac{200}{1.5} = 262\,233 \text{ daN}$$

$$N_{\text{pl.Rk}} = A_a f_y + A_c f_{\text{ck}} = 77 \cdot 2350 + 733 \cdot 200 = 327\,550 \text{ daN}$$

$$(EI)_e = E_a I_a + 0.6 \cdot E_{\text{cm}} I_c = 2.1 \cdot 10^6 \cdot 17\,624 + 0.6 \cdot 0.29 \cdot 10^6 \cdot 109\,442 = 56.05 \cdot 10^9 \text{ daN} \cdot \text{cm}^2$$

$$N_{\text{cr}} = \frac{\pi^2 (EI)_e}{L^2} = \frac{\pi^2 \cdot 56.05 \cdot 10^9}{800^2} = 863\,485 \text{ daN}$$

$$\bar{\lambda} = \sqrt{\frac{N_{\text{pl.Rk}}}{N_{\text{cr}}}} = 0.62 \Rightarrow \chi = 0.82 \quad (\text{curve b})$$

The column design resistance to axial compression will be:

$$N_{\text{Rd}} = \chi \cdot N_{\text{pl.Rd}} = 0.82 \cdot 262\,233 = 215\,031 \text{ daN} = 2150 \text{ kN}$$

- **Type B:**

According to EC 3:

For cross-section Class 1 the design resistance will be:

$$N_{Rd} = \chi \cdot A_g \frac{f_y}{\gamma_{M1}}$$

It is evaluated:

$$\lambda = \frac{L}{i_y} = \frac{800}{15.13} = 52.88; \quad i_y = \sqrt{\frac{I_y}{A_g}} = \sqrt{\frac{17624}{77}} = 15.13 \text{ cm}; \quad \beta_A = \frac{A_{eff}}{A_g} = 1$$

$$\bar{\lambda} = \frac{\lambda}{\lambda_1} \sqrt{\beta_A} = \frac{52.88}{93.9} = 0.563; \quad \lambda_1 = \pi \sqrt{\frac{E}{f_y}} = 93.9 \cdot \varepsilon = 93.9; \quad \Rightarrow \chi = 0.86$$

It results the steel column design resistance:

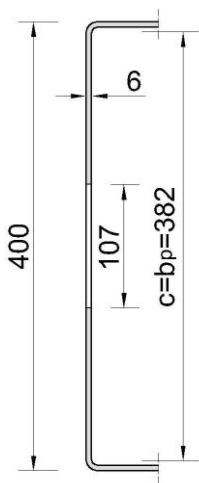
$$N_{Rd} = \chi \cdot A_g \frac{f_y}{\gamma_{M1}} = 0.86 \cdot 77 \frac{2350}{1.1} = 141470 \text{ daN} = 1415 \text{ kN}$$

- **Type C:**

According to EC 3:

Effective cross-section:

– the large wall panel (web): $h=400 \text{ mm}$ (Fig.4):

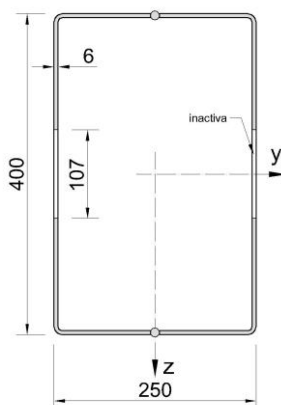


$$\frac{c}{t} = \frac{400 - 3 \cdot 6}{6} = 63.67; \quad c = b_p = h - 3 \cdot t = 382 \text{ mm}$$

$$\bar{\lambda}_p = \frac{b_p / t}{28.4 \cdot \varepsilon \cdot \sqrt{k_\sigma}} = \frac{63.67}{28.4 \cdot 1 \cdot \sqrt{4}} = 1.12 > 0.673$$

$$\rho = \frac{\bar{\lambda}_p - 0.22}{\bar{\lambda}_p^2} = \frac{1.12 - 0.22}{1.12^2} = 0.72 \Rightarrow b_{eff} = \rho \cdot b_p = 0.72 \cdot 382 = 275 \text{ mm}$$

Fig. 4.



– the flange ($b=250 \text{ mm}$):

$$\frac{c}{t} = \frac{250 - 3 \cdot 6}{6} = 38.67; \quad c = b_p = b - 3 \cdot t = 232 \text{ mm}$$

$$\bar{\lambda}_p = \frac{b_p / t}{28.4 \cdot \varepsilon \cdot \sqrt{k_\sigma}} = \frac{38.67}{28.4 \cdot 1 \cdot \sqrt{4}} = 0.68 \approx 0.673$$

$$\rho = \frac{\bar{\lambda}_p - 0.22}{\bar{\lambda}_p^2} = \frac{0.68 - 0.22}{0.68^2} = 0.99 \approx 1 \Rightarrow b_{eff} \approx b_p = 232 \text{ mm}$$

The effective cross-section is presented in Figure 5.

$$A_{a,eff} = 76.5 - 2 \cdot 10.7 \cdot 0.6 = 63.66 \text{ cm}^2$$

$$I_{a,eff} = 17485 - 2 \frac{0.6 \cdot 10.7^3}{12} = 17362 \text{ cm}^4$$

Fig. 5.

According to EC 4, adapted for Class 4 cross-section:

$$N_{pl,Rd} = A_{a,eff} \frac{f_y}{\gamma_a} + A_c \frac{f_{ck}}{\gamma_c} = 63.66 \frac{2350}{1.1} + 804 \frac{200}{1.5} = 243200 \text{ daN}$$

$$N_{pl,Rk} = A_{a,eff} f_y + A_c f_{ck} = 63.66 \cdot 2350 + 804 \cdot 200 = 310401 \text{ daN}$$

$$(EI)_e = E_a I_{a,eff} + 0.6 \cdot E_{cm} I_c = 2.1 \cdot 10^6 \cdot 17362 + 0.6 \cdot 0.29 \cdot 10^6 \cdot 115848 = 56.6 \cdot 10^9 \text{ daN} \cdot \text{cm}^2$$

$$N_{cr} = \frac{\pi^2 (EI)_e}{L^2} = \frac{\pi^2 \cdot 56.6 \cdot 10^9}{800^2} = 871958 \text{ daN}$$

$$\bar{\lambda} = \sqrt{\frac{N_{pl,Rk}}{N_{cr}}} = 0.60 \Rightarrow \chi = 0.84 \quad (\text{curve b - welded section})$$

It results the design resistance of the axial compression composite column:

$$N_{Rd} = \chi \cdot N_{pl,Rd} = 0.84 \cdot 243200 = 204288 \text{ daN} = 2043 \text{ kN}$$

- **Type D:**

The cross-section is of Class 4, so the effective area will be used to evaluate the column design resistance:

It is calculated:

$$\lambda = \frac{L}{i_y} = \frac{800}{15.12} = 52.9; \quad i_y = \sqrt{\frac{I_y}{A_g}} = \sqrt{\frac{17485}{76.5}} = 15.12 \text{ cm};$$

$$\beta_A = \frac{A_{eff}}{A_g} = \frac{63.66}{76.5} = 0.832$$

$$\bar{\lambda} = \frac{\lambda}{\lambda_1} \sqrt{\beta_A} = \frac{52.9}{93.9} \sqrt{0.832} = 0.51; \quad \lambda_1 = \pi \sqrt{\frac{E}{f_y}} = 93.9 \cdot \varepsilon = 93.9; \quad \Rightarrow \chi = 0.88$$

The design resistance of the steel column will be:

$$N_{Rd} = \chi \cdot A_{eff} \frac{f_y}{\gamma_{M1}} = 0.88 \cdot 63.66 \frac{2350}{1.1} = 119680 \text{ daN} = 1197 \text{ kN}$$

The results containing the design resistances of the analyzed columns are centralized in Table 1.

Table 1.

COLUMN TYPE	A	B	C	D
N_{Rd} [kN]	2150	1415	2043	1197

Table 2. presents suggestively the efficiency ratio for the analysed cross-section types.

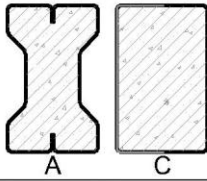
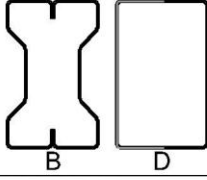
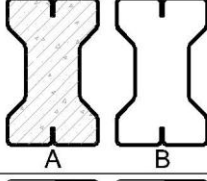
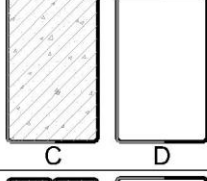
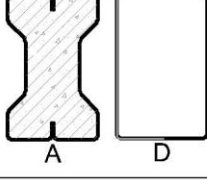
Caz	SECTIUNI COMPARATE	RAPORT INTRE REZISTENTE
1		1,05
2		1,18
3		1,52
4		1,70
5		1,80

Table 2.

4. CONCLUSIONS

The thin-walled members can offer advantageous solutions for composite concrete-filled hollow steel sections taking into account the following considerations:

- a large variety of cross-section types can be obtained using thin-walled members;
- a good esthetical aspect can be obtained using TWM;
- welded lipped edges and folded shape increases the cross-section rigidity having the function of longitudinal stiffeners;
- the simple solutions of joints with the adjacent elements can be obtained.

REFERENCES

- [1] Moga,P., Păcurar,V.,Guțiu,Șt.,Moga,C.: Calculul elementelor metalice. Norme române-Eurocode 3. UT.PRES. Cluj-Napoca. 2006.
- [2] Moga,P., Moga,C. Guțiu,St.,Câmpean,Cr.: Design of axial compression members according to European codes. Proceedings of the International Conference in Metal Structures. Poiana Brașov, România, sept. 2006.
- [3] Păcurar,V., Moga, C., Guțiu, St., Câmpean, C.: Design of composite columns in accordance with Eurocode 4. Proceedings of the International Conference in Metal Structures. Poiana Brașov, România, sept. 2006.
- [4] Păcurar,V., Moga, C., Guțiu, St., Câmpean, C.: Calculul stâlpilor cu secțiune mixtă oțel-beton în conformitate cu normativul Eurocode 4. Acta Technica Napocensis, Nr. 48 / 2005.

*** EUROCODE 3. Design of steel structures. EN 1993.

*** EUROCODE 4. Design of composite concrete and steel constructions. EN 1994.

The Influence of Composite Column Slenderness on the Confinement Effect

Az együttdolgozó-öszvérkeresztmetszetű oszlopok karcsúságának a hatása a beton keresztirányú alakváltozását gátló jelenség együtthatójára

Influența zvelteții stâlpului cu secțiune compozită asupra factorului de confinare

Petru MOGA, Gavril KÖLLŐ, Ștefan GUȚIU, Cătălin MOGA

Railway Bridge Department at the Technical University of Cluj-Napoca, Romania,
Civil Engineering Faculty

ÖSSZEFOGLALÓ

Mivel a beton keresztirányú alakváltozását (deformációját) az acélkeresztmetszet (az acélcső) megátolja, így a beton oldalirányú alakváltozása nem jöhet létre. Tehát az acél csőben megnő a beton nyomófeszültsége és csökken az acél feszültsége a kétirányú feszültségállapot miatt.

Ebben a tanulmányban elemzésre kerül a körkeresztmetszetű öszvéroszlop karcsúságának a hatása kétirányú feszültség változására, vagyis a beton „konfinációjára”.

Ennek a paraméternek a változását hivatott bemutatni a tanulmányban közölt gyakorlati alkalmazás amelynek az eredményei hozzásegítenek bizonyos következtetések megtételéhez és a jelenség jobb megértéséhez.

REZUMAT

Datorită deformației laterale a betonului, împiedicată să se producă liber de către tubul metalic cu caracteristici mecanice superioare, apare fenomenul de confinare a betonului din interiorul tubului metalic, constând în mărirea rezistenței la compresiune, simultan producându-se micșorarea rezistenței oțelului datorită stării de tensiune plane în care se află acesta.

În lucrare se analizează influența zvelteții stâlpului cu secțiune compusă oțel-beton circulară, asupra efectului de confinare a betonului. Efectul acestui parametru este exemplificat printr-o aplicație numerică, care a permis formularea unor observații utile pentru înțelegerea și utilizarea în proiectare a fenomenului de confinare.

ABSTRACT

In a composite column consisting of a concrete-filled hollow steel section, the circular steel tube encloses the concrete core; hence, lateral compressive confining stresses on the concrete are induced by the confinement provided by the steel tube.

This paper presents the confinement assessment in accordance with Eurocode 4 norm and the working example analyzes the influence of the column relative slenderness on the confinement factor and on the load carrying capacity of a circular composite column subjected to axial compression.

Some useful remarks on the design activity of such members are also presented in this paper.

1. CONFINEMENT EFFECT ACCORDING TO EC 4

Eurocode 4 norm takes into account the confinement effect for circular composite columns by increasing the characteristic resistance of the structural concrete with the confinement factor noted here with C^* :

$$C^* = \left(1 + \eta_c \frac{t f_y}{d f_{ck}} \right) \quad (1)$$

where:

$$\eta_c = \eta_{co} \left(1 - \frac{10e}{d} \right) \quad (2.a)$$

$$\eta_{co} = 4.9 - 18.5 \bar{\lambda} + 17 \bar{\lambda}^2 \geq 0 \quad (2.b)$$

The confinement effect is not taken into account when:

$$\bar{\lambda} < 0.5 \text{ or } e < \frac{d}{10}; \quad e = \frac{M_{Ed,max}}{N_{Ed}} - \text{eccentricity of the axial force;}$$

where: $\bar{\lambda} = \sqrt{\frac{N_{pl,Rk}}{N_{cr}}}$ - relative slenderness

in which:

$$N_{pl,Rk} = A_a f_y + A_c f_{ck} + A_s f_{sk}$$

$$N_{cr} = \frac{\pi^2 (EI)_e}{l^2}$$

$(EI)_e$ – elastic flexural stiffness:

$$(EI)_e = E_a I_a + 0.6 E_{cm} I_c + E_s I_s$$

I_a ; I_c ; I_s – second moment of area of the structural steel section, the un-cracked concrete section and reinforcement;

E_a ; E_s – modulus of elasticity of structural steel and reinforcement;

E_{cm} – secant modulus of elasticity of concrete.

The following condition has to be fulfilled:

$$0.2 \leq \delta = \frac{A_a \cdot f_y / \gamma_a}{N_{pl,Rd}} \leq 0.9 \quad (3)$$

If the steel contribution ratio, $\delta < 0.2$, the column will be designed as a concrete column and when $\delta > 0.9$, the column will be designed as a steel column.

To avoid the local buckling of the steel tube wall the following condition also has to be fulfilled:

$$\frac{d}{t} \leq 90 \varepsilon^2; \quad \varepsilon = \sqrt{\frac{235}{f_y}} \quad (4)$$

In the case when the relative slenderness is high, respectively $\bar{\lambda} > 0.5$, the confinement effect cannot be taken into account because the compression column failure takes place through the general buckling and in the structural concrete the strength f_{ck} cannot be reached (the confinement effect can be developed only when $\sigma_c > f_{co}$ (respectively f_{ck})).

Also in the case of high eccentricity of the axial load, $e > d/10$, only part of concrete core is subjected to compression and the confinement effect cannot be taken into consideration.

In the Eurocode 4, full composite action up to maximum load resistance is assumed in the design of composite columns which means strain compatibility between the steel section and the concrete core, and consequently no slip should occur in the interface between the concrete and the steel tube.

In accordance with EC 4 norm, the plastic resistance of a composite circular column (without reinforcement), and subjected to axial compression is given by the relation:

$$N_{pl,Rd} = \eta_a A_a f_y \frac{1}{\gamma_a} + A_c \frac{f_{ck}}{\gamma_c} \left(1 + \eta_c \frac{t f_y}{d f_{ck}} \right) \quad (5)$$

where η_a is the coefficient which takes into account the diminishing of the steel strength caused by the biaxial state of stresses:

$$\eta_a = \eta_{a0} + (1 - \eta_{a0}) \frac{10 e}{d} \quad (6.a)$$

$$\eta_{a0} = 0.25 \left(3 + 2\bar{\lambda} \right) \leq 1 \quad (6.b)$$

The load carrying capacity (resistance capacity) of the axial compression composite column is:

$$N_{Rd} = \chi \cdot N_{pl,Rd} \quad (7)$$

The reduction factor: $\chi = \frac{1}{\phi + \sqrt{\phi^2 - \bar{\lambda}^2}}$; $\chi \leq 1$

where: $\phi = 0,5 \left[1 + \alpha(\bar{\lambda} - 0,2) + \bar{\lambda}^2 \right]$; $\alpha = 0.21$ - imperfection factor-curve *a*

2. WORKING EXAMPLE

The influence of the composite column slenderness on the confinement effect and on the load carrying capacity is analyzed in this example

Column cross-section and design characteristics (Fig.1)

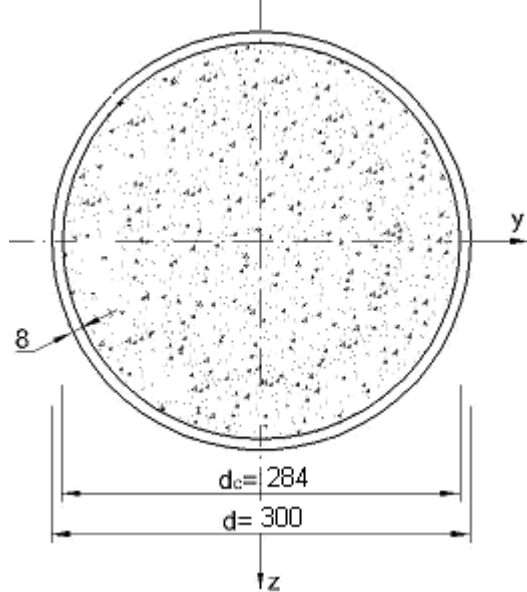


Fig. 1.

Steel component::

Steel pipe: 300 × 8 mm
- Steel S 355

- $f_y = 355 \text{ N/mm}^2$
- $E_a = 210\,000 \text{ N/mm}^2$
- $\gamma_a = 1.1$
- $A_a = 73.4 \text{ cm}^2$
- $I_a = 7\,828 \text{ cm}^4$

Concrete: Class C 25/30:

- $f_{ck} = 25 \text{ N/mm}^2$
- $E_{cm} = 30\,500 \text{ N/mm}^2$
- $\gamma_c = 1.5$
- $A_c = 633 \text{ cm}^2$

$$I_c = \frac{\pi d_c^4}{64} = \frac{\pi \cdot 28.4^4}{64} = 31933 \text{ cm}^4$$

The condition to apply the EC 4 design method:

$$N_{pl,Rd} = 73.4 \frac{3550}{1.1} + 633 \frac{250}{1.5} = 342382 \text{ daN}$$

$$A_a f_y / \gamma_a = 73.4 \cdot 3550 / 1.1 = 236\,882 \text{ daN}$$

- $0.2 < \delta = 236\,882 / 342\,382 = 0.69 < 0.9$
- $d/t = 300/8 = 37.5 < \max(d/t) = 90 \text{ (} 235/355 \text{)} = 59.6$

The column elastic flexural stiffness is:

$$(EI)_e = 2.1 \cdot 7828 \cdot 10^6 + 0.6 \cdot 0.305 \cdot 31933 \cdot 10^6 = 22283 \cdot 10^6 \text{ daN} \cdot \text{cm}^2$$

It is calculated $N_{pl,Rk}$:

$$N_{pl,Rk} = 73.4 \cdot 3550 + 633 \cdot 250 = 418\,820 \text{ daN}$$

The elastic critical failure force:

$$N_{cr} = \frac{\pi^2 22\,283 \cdot 10^6}{L^2} = \frac{2.20 \cdot 10^{11}}{L^2} \text{ daN}$$

The relative slenderness $\bar{\lambda}$:

$$\bar{\lambda} = \sqrt{\frac{N_{pl,Rk}}{N_{cr}}} = L \sqrt{\frac{418\,820}{2.20 \cdot 10^{11}}} = 1.38 \cdot 10^{-3} \cdot L$$

The column length corresponding to slenderness $\bar{\lambda}$:

$$L = 725 \cdot \bar{\lambda} \text{ [cm]} = 7.25 \cdot \bar{\lambda} \text{ [m]}$$

The confinement factor:

$$C^* = \left(1 + \eta_c \frac{t f_y}{d f_{ck}} \right) = \left(1 + \eta_c \frac{8 \cdot 355}{300 \cdot 25} \right) = 1 + 0.378 \cdot \eta_{co}$$

where:

$$\eta_c = \eta_{co} \left(1 - \frac{10e}{d} \right) = \eta_{co} \text{ - for } e=0$$

$$\eta_{co} = 4.9 - 18.5 \bar{\lambda} + 17 \bar{\lambda}^2 \geq 0$$

The plastic resistance taking into account de confinement factor will be:

$$N_{pl,Rd} = \eta_a A_a f_y \frac{1}{\gamma_a} + A_c \frac{f_{ck}}{\gamma_c} \left(1 + \eta_c \frac{t f_y}{d f_{ck}} \right) = 236\,882 \cdot \eta_a + 105\,500 \cdot C^* \text{ [kN]}$$

where η_a is the coefficient which takes into account the diminishing of the steel strength caused by the biaxial state of stresses:

$$\eta_a = \eta_{ao} + (1 - \eta_{ao}) \frac{10e}{d} = \eta_{ao} \text{ - for } e = \frac{M_{Sd,max}}{N_{Sd}} = 0$$

$$\eta_{ao} = 0.25 \left(3 + 2\bar{\lambda} \right) \leq 1$$

In Table 1 the calculation results are centralized.

The relation between the load carrying capacity and the column relative slenderness is presented in figure 2.

Table1

No.	$\bar{\lambda}$	L [m]	η_{co}	C*	η_{ao}	$N_{pl,Rd}$ [kN]	χ	$\chi \cdot N_{pl,Rd}$ [kN]
1	0	0	4.90	2.85	0.75	4 783	1	4 783
2	0.10	0.725	3.22	2.22	0.80	4 237	1	4 237
3	0.15	1.087	2.50	1.95	0.82	4 012	1	4 012
4	0.20	1.450	1.88	1.71	0.85	3 818	1	3 818
5	0.25	1.810	1.34	1.50	0.87	3 655	0.98	3 582
6	0.30	2.175	0.88	1.33	0.90	3 535	0.97	3 429
7	0.35	2.537	0.51	1.19	0.92	3 447	0.96	3 309
8	0.40	2.900	0.22	1.08	0.95	3 390	0.95	3 220
9	0.45	3.260	0	1	0.97	3 365	0.93	3 129
10	0.50	3.625	0	1	1	3 424	0.92	3 150
11	0.60	4.350	0	1	1	3 424	0.89	3 047
12	0.70	5.075	0	1	1	3 424	0.85	2 910
13	0.80	5.800	0	1	1	3 424	0.80	2 739
14	1.00	7.250	0	1	1	3 424	0.66	2 260

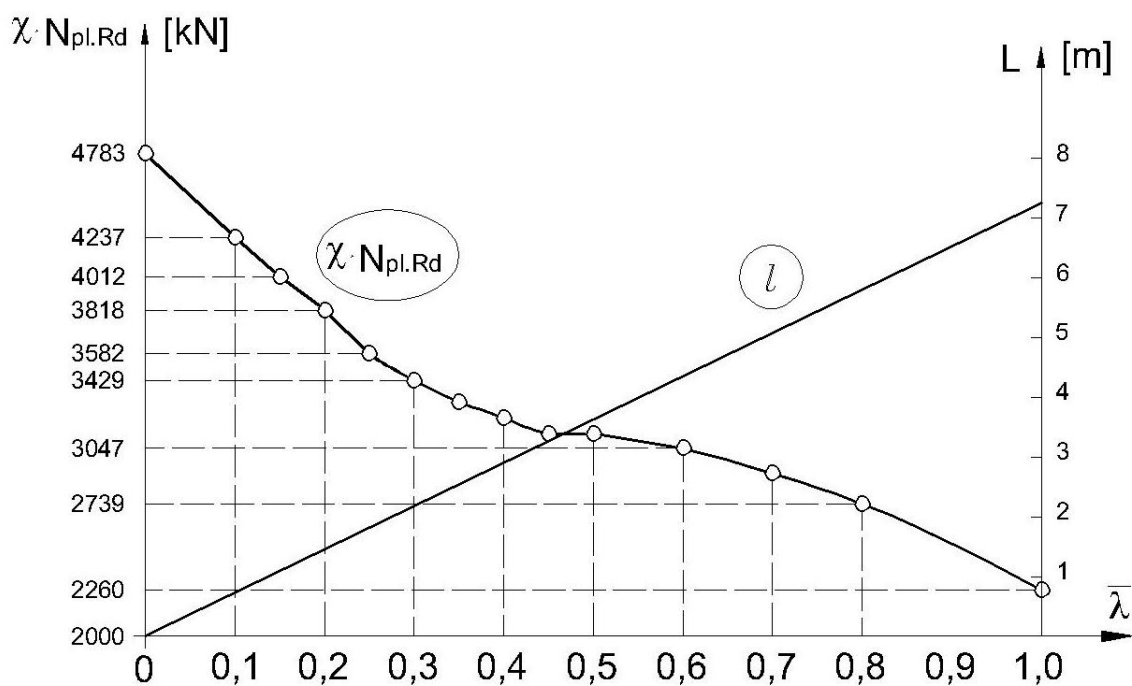


Fig. 2.

3. FINAL REMARKS

By analyzing the confinement phenomenon and from the presented working example, some useful observations and remarks about the design activity of the composite circular columns can be made:

GENERAL REMARKS:

- the confinement effect increases when the steel tube thickness is higher;
- the confinement effect is diminishing when the steel tube diameter increases;
- the high-strength structural steel induces a higher confinement effect on the concrete core in comparison with the normal-strength steel;

- the confinement effect is more substantial in case of normal-strength concrete (NSC) in comparison with high-strength concrete (HSC);
- the confinement effect is not taken into account when the axial load eccentricity, $e > d / 10$;
- the confinement effect is vanishing when the relative slenderness of the composite column, $\bar{\lambda} > 0.45$;
- the state of stresses of a composite column is complex, so, in structural concrete there is a spatial state of stresses and in the tube steel there is a biaxial state of stresses.

REMARKS RESULTED FROM THE WORKING EXAMPLE:

- the confinement effect increases characteristic resistance of the concrete by 8% for $\bar{\lambda} = 0.40$, up to 2.85 higher for $\bar{\lambda} = 0$ in comparison with unconfined concrete;
- the diminishing of the steel strength caused by the biaxial state of stresses is between 0.75...0.95.

REFERENCES

- [1.] Bergmann,R., Matsui,C., Meinsma,C., Dutta,D.: Design guide for concrete-filled hollow section columns under static and seismic loading. Verlag TUV Rheinland Koln.1995.
- [2.] Grauers, M: Composite Columns of Hollow Sections Filled with High Strength Concrete. Chalmers University of Technology. Goteborg. 1993.
- [3.] Lawson,R.M.,Wickens,P.: Steel Designer Manual (6th Edition). Chapter 22: Composite columns. 2001.
- [4.] Moga,C.: Cercetări pe stâlpi cu secțiune mixtă oțel-beton. Referat de doctorat. UT Cluj-Napoca.2007.
- [5.] *** ESDEP WG 10. Composite construction. Lecture 10.
- [6.] *** EC 3. Design of steel structures. EN 1993.
- [7.] *** EC 4. Design of composite concrete and steel constructions. EN 1994.
- [8.] *** SR EN 1994-1-1/2004. Proiectarea structurilor compozite de oțel și beton.

Presence of Chloride Ions in Concrete

Kloridionok a betonban

Ionii de clorid în beton

Katalin KOPECSKÓ

Budapest University of Technology and Economics
Department of Construction Materials and Engineering Geology
H-1111 Budapest, Műegyetem rkp. 3.
Tel: +36 1 463 4068, fax: +36 1 463 2017
katalin@eik.bme.hu, honlap: www.eat.bme.hu

ÖSSZEFOGLALÓ

A kloridionok többféle módon kerülhetnek a betonba: alkotóelemeik által készítéskor (pl. az adalékanyaggal vagy adalékszerrel), a jégtelenítő sózás vagy a tengermelléki környezet által, illetve tüzeset során a PVC bomlásából. Az elmúlt évtizedekben a jégtelenítő sózás alkalmazása jelentős korróziós károkat okozott. Világszerte kutatásokat folytatnak a korróziós mechanizmus megértése céljából, hogy megvédhessék az acélbetéteket a korróziótól és, hogy a felújítások elkerülhetőek legyenek. Fontos kérdés a cementek által megköthető kloridtartalom, illetve a kloridkötés körülményeinek tisztázása. Másfelől fontos meghatározni az acélbetét korrózióját kiváltó feltételeket is. Jelen cikk összefoglalja a Budapesti Műszaki és Gazdaságtudományi Egyetem Építőanyagok és Mérnökgeológia Tanszékének ezen a téren folytatott évtizedes múltú kutatásait.

REZUMAT

Ionii de clor pot ajunge în mai multe modalități în beton, de exemplu cu materiale de adaos, prin așternerea sărurilor utilizate pentru eliminarea ghețurilor, prin descompunerea PVC-ului.

În ultimii ani utilizarea sărurilor pentru topirea zăpezii și a ghețurilor a generat coroziune în betoane.

În toată lumea se fac cercetări pentru deslușirea mecanismelor de coroziune, pentru protejarea armăturilor împotriva coroziunii.

Lucrarea sintetizează cercetările efectuate de catedra de „materiale de construcții și geologie inginerească” a Universității Tehnice și Economice din Budapesta.

ABSTRACT

Chloride ions may be present in concrete from its constituents, from de-icing salts, from seawater or from PVC due to fire. In the last decades application of de-icing salts induced considerable corrosion of steel reinforcement. Researches were directed to understand the mechanism of corrosion in order to be able to avoid corrosion and repair of corroded members. One of the major issues is to find the critical chloride content that can be bound by various cements and the way of chloride binding. On the other hand it is important to define the circumstances the initiation of steel reinforcement's corrosion. Present paper summarises the test results on chloride ion binding capacity in concrete carried out at the Department of Construction Materials and Engineering Geology, Budapest University of Technology and Economics in the last couple of years.

Keywords: Corrosion, steel reinforcement, de-icing salts, chloride ion binding, Kuzel's salt, Friedel's salt

1. INTRODUCTION

Chlorides may be present in concrete due to the following reasons:

- during preparation mixed together with the constituents (cement, aggregate, water and admixture)
- during its lifetime:

- by using de-icing salts
- originating from seawater
- produced during fire (e.g. decomposition of PVC).

Herewith we deal only with two cases.

1.1. Chlorides originating from the constituents

Admixtures, which include CaCl_2 , were used to increase the hydration rate of cements. Its typical example was in Hungary the Tricosal SIII admixture before the Second World War (Balázs, 1996a). In order to avoid CaCl_2 induced corrosion, Kalcidur NV admixture came into use after the War that included CaCl_2 as well as NaNO_2 inhibitor in the same amount.

In case of a special construction system (called IMS), prestressing tendons deteriorated due to the chloride content of the injecting mortar. Principle idea of the IMS system is that concrete slabs are prestressed against concrete columns by post tensioned tendons in two directions. After prestressing the channels of tendons were filled with PU mortar, which included calcium chloride. CaCl_2 induced corrosion of prestressing tendons of IMS structures (Balázs, 1996b).

1.2. Chlorides originating from de-icing salts

Despite the strict regulations of environmental protection, NaCl as de-icing salt is often used in several countries during wintertime. Couple of researches was directed to substitute NaCl with other de-icing agents; however, efficient and economic solution is still not available.

Chlorides from de-icing salts reach the concrete members dissolved in molten ice or snow but also with splashed or sprayed water.

Chloride transport in hardened concrete occurs through the capillarity by the pore water; therefore, the capillary system of concrete has a major importance.

2. IMPORTANCE OF CHLORIDES IN THE PROCESS OF CORROSION OF REINFORCEMENT

One of the reasons of widespread use of reinforced concrete is the passive layer on the surface of reinforcement produced by the high alkalinity ($\text{pH} \sim 12$) during the hydration of cement. This layer protects the reinforcement from corrosion (Balázs-Tóth, 1997).

Corrosion can start even without chlorides whenever the following three conditions are simultaneously fulfilled:

- alkalinity of concrete is lost due to carbonation ($\text{pH} \leq 9$)
- water is available in the capillary pores
- oxygen is available nearby the reinforcement after penetration through the concrete cover.

Presence of chloride ions changes the type of corrosion from surface corrosion to pitting corrosion.

Chloride ions absorb water which increases the electric conductivity of concrete around the reinforcement (electrochemical corrosion). Chlorides will not be bound in carbonated concrete.

3. CHLORIDE ION BINDING IN GENERAL

Researchers agree in that *only those chloride ions induce corrosion, which are not bound chemically and are in the pore water as a solution*. However, researchers disagree in how and how much chlorides can be bound.

It is known more than 100 years that chloride ions originated from accelerator (CaCl_2), which are present dissolving by mixing water of the constituents of concrete, will be bound in form of Friedel's salt named after it's discoverer (Friedel, 1897):



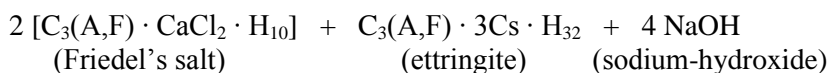
According to the above formula CaCl_2 react with the aluminat clinker mineral (C_3A) of cement. This type of chloride binding mechanism was supported by our experiments to increase the hardening (Balázs, 2001). Our experiments also indicated that the amount of bound chloride ions might be less after the steam-curing of concrete.

The form of Friedel's salt did not give answer why sulphate resistant cement (CEM I 32.5 S) binds chloride ions, without C₃A clinkers.

Application of de-icing salts differs from the above situation in two ways:

- NaCl is used instead of CaCl₂
- age of concrete is at least one month (e.g. by the opening of a bridge). By this time hydrates are formed from the constituents of cement. In order to be able to bind the chlorides of de-icing salts, any of the hydrates are needed to be dissolved.

Volkwein (1987) assumed the following mechanism, based on the investigation of 22 years old bridges:



According to this equation:

- monosulphate dissolves
- Friedel's salt is produced both from C₃A and C₄AF
- ettringite is re-established from monosulphate
- sodium-hydroxide (NaOH) is released, which increases the probability the alkali-aggregate reaction.

Chloride ion content of concrete can be determined by the classic Mohr method and the chloride content (bound and free) should be related to the cement content, since only the cement clinkers can bind chloride ions.

The considerable amount of chloride induced corrosion led to research on the circumstances of chloride corrosion. On the other hand research started in two directions to avoid corrosion of reinforcement:

- to determine the maximum amount of chlorides to be bound and the circumstances of binding of the chlorides
- to determine the amount of chlorides that start to induce corrosion. This amount is considered to be the allowable chloride content (Breit, 2001).

Comparison of test results is often difficult because the type of cements and measuring methods differ. A series of measurements by Lukas (1983) indicating considerable differences in chemically bound chloride contents in the function of the cement type. Lukas considered the chloride content to be bound, which is soluble in alcohol.

4. RESEARCH AT THE DEPARTMENT OF CONSTRUCTION MATERIALS

4.1. Chloride binding capacity of C₃A, C₄AF and C₃S clinkers

Interaction of chloride ions and cements can be modelled by studying directly the interaction of chloride ions and the clinker minerals. Reason of research was to study how clinkers bind NaCl (Hungarian Research Found, OTKA 3000). In one part of the experiments NaCl was added to the samples during mixing, while in the other part of the experiments the hardened samples were immersed into chloride solution in various ways or the samples were sprayed with NaCl solution, respectively.

Samples of 10×10×50 mm were prepared with C₃A, C₄AF and C₃S clinker minerals. The samples made us possible to have a strength analysis record for every chemical investigation by cutting 10 mm slices. The investigations took place at ages of 1, 28 56 90 and 180 days. Investigation methods were thermal (TG, DTG, DTA) and X-ray diffraction analyses as well as splitting strength analysis.

Summary of the test results (Balázs-Csizmadia-Kovács, 1997):

Both C₃A and C₄AF bind chlorides in the form of monochloro-aluminate-hydrate (Friedel's salt) or monochloro-ferrite-hydrate. Analogous aluminate or ferrite hydrates form solid solution with each other. *Thermal and X-ray analysis showed that chloride ions either from NaCl added to the mixing water or penetrated from outer source into the already settled cement can be bound in the presence of either C₃A or C₄AF to form C₃A · CaCl₂ · 10H₂O or C₃F · CaCl₂ · 10H₂O (Fig. 4).*

Test results also indicated that binding of NaCl was possible even in hardened specimens. Only the chloride ions of NaCl will be bound in the hydrates while the Na⁺ ions increase the alkali content of the pore water. Water content of samples treated anyhow with NaCl (added to the mixing water or after hardening) was 5 to 6 % higher than that of non-treated samples due to the strong hygroscopic property of NaCl.

Chloride ion binding capacity of C_3S was also investigated. The preparation and the salt treatment were the same as in case of C_3A . NaCl added to the C_3S increases the hydration rate. Even X-ray diffraction analysis did not detect any sign of chloride building into the crystal structure of calcium-silicate-hydrate. *However, all samples treated with NaCl showed an increase in their water content because hydration in the beginning phase of the reaction was reasonably fast.* Even if the literature reports only about chloride ions that are bound in C-S-H with secondary forces it is possible that NaCl not only increase the rate of reaction but perhaps it influences the structure of C-S-H. Because of the temperature range of 550 to 670 °C (which is indicated in the literature as dehydration of C-S-H) we observed DTG peaks at 580 and 630 °C.

4.2. Chloride binding capacity of cements

Next question within the above research (Hungarian Research Found, Grant OTKA 3000) was if binding of chloride ions were possible also in cements, which are more complex than clinkers contributing to the durability of concrete. Heterogeneity of cements and variation in the quality of the clinkers make to find the answer rather difficult. Even in this case a general picture of chloride binding capacity of cements is necessary. Specimens were subjected to salt treatment from 1 to 28 or 28 to 56 days and studied with X-ray diffraction and thermal tests (Derivatograph).

Summary of the observations is the following (Balázs, 2001):

Both X-ray patterns and derivatograms indicated that the chloride ions of NaCl will be bound by C_3A and C_4AF in form of $C_3A \cdot CaCl_2 \cdot 10H_2O$ or $C_3F \cdot CaCl_2 \cdot 10H_2O$.

Production of $C_3A \cdot CaCl_2 \cdot 10H_2O$ was observed by all of the investigated cements, which were treated by NaCl during hydration.

$C_3A \cdot CaCl_2 \cdot 10H_2O$ was produced either from hexagonal calcium-aluminate-hydrates [$C_3A \cdot Ca(OH)_2 \cdot 12H_2O$, $C_3A \cdot CaSO_4 \cdot 12H_2O$] by the substitution of anions or was directly produced during hydration reacting with C_3A , but it is hard to be predicted from the reaction $2NaCl + Ca(OH)_2 \rightarrow CaCl_2 + 2NaOH$. It was also observed that $C_3A \cdot CaCl_2 \cdot 10H_2O$ can be produced after 28 days (i.e. after hardening) by NaCl treatment.

Amount of $C_3A \cdot CaCl_2 \cdot 10H_2O$ is mainly determined by the content of C_3A and C_4AF of the cement considering constant concentration of NaCl solution.

We were not able to detect calcium-silicate-hydrates by X-ray, which include chlorides. According to the literature, it was not yet possible to show if the chloride ions are chemically bound by primary forces. Chloride ions are possibly bound by chemisorptions. Type of binding was not detectable in our tests. *Fly ash did not have a considerable influence on chloride binding. Binding of chlorides was observed only with C_3A and C_4AF clinkers.*

Chloride binding capacities of the investigated cements are in decreasing rate the following (highest capacity first and lowest capacity last):

- CEM I 42.5 R
- CEM II A-V 32,5 (20 m% fly ash content)
- CEM I 32,5 S (sulphate resistant PC).

4.4. Chloride ion binding capacity of steam cured concretes

Large portion of concrete structures in Hungary is made out of steam cured concrete. Steam curing is a generally used method in the production of precast concrete elements. Increased temperature accelerates the hydration resulting high early strength. However, accelerated curing affects detrimentally both the long-term strength and the durability. Hooton and his colleges (2004) concluded that steam-cured concretes containing silica fume or blends both of silica fume and ground granulated blast-furnace slag exhibit improved chloride penetration resistance compared to those of Portland cement concretes.

Dhir and his co-authors (1996) reported the results of chloride binding measurements of GGBS pastes, as well as chloride diffusion and permeability measurements of GGBS concrete mixes. They found that in concrete designed to have a minimum volume of voids, the chloride ion binding capacity of the cement matrix becomes the dominant factor in how resistant the concrete is to chloride permeation. Luo and his colleges (2003) experimentally studied both the chloride diffusion coefficient and the chloride binding capacity of Portland cement or blended cement made of Portland cement and 70 % GGBS replacement with or without 5 % sulphate. They found that (i) chloride diffusion coefficient decreased; (ii) chloride ion binding capacity improved in samples of blended cement. Moreover the chloride ion binding capacity was lower in case of samples containing 5 % sulphate.

Our last experimental programme was directed to study the chloride binding capacity of steam cured cement stones (Hungarian Research Found, Grant OTKA T034467). Purpose of research was to answer the following questions:

- What is the effect of the different kind and amount of mineral additives on the chloride ion binding of cements? Chloride ion binding capacity of cements was investigated in the function of test parameters.
- What is the influence of the curing temperature (natural hardening at 20°C, or steam curing at 80°C) on the hydration processes of cements?

Hydration process was studied by thermal test (DTA/TG/DTG) using Derivatograph Q-1500 D and X-ray diffraction (XRD) using Philips PW 3710 diffractometer. Simultaneous application of thermoanalytical methods and powder diffraction made possible to carry out detailed analysis of phase modifications. Research included the determination of

- types of hydrates by X-ray diffractometry and thermal test (TG, DTG, DTA)
- the chloride content bounded in form of Friedel's salt

Four types of cements were selected with different slag contents and ordinary Portland cement as a reference material, respectively. Sulphate contents of cements were not modified (hence the influence of various sulphate contents was not studied separately for the cements). Samples of cements were prepared by the required amount of water to reach the standard consistence (semi-plastic) (MSZ EN 196-3) (Tab. 1).

Table 1. Cement types

Cements	Additive	w/c
CEM I 42.5 N (OPC)	0 m%	0.273
CEM II/B-M (V-L) 32,5 R	18 m% V, 10 m% L	0.270
CEM II/B-S 32.5 R	26 m% GGBS	0.272
CEM III/A 32.5 N	40 m% GGBS	0.285
CEM III/B 32.5 N-S	62 m% GGBS	0.302

Tests were carried out to study the influence of salt treatment and steam curing (Tab. 2).

Table 2. Experimental programme

Series	Curing and exposure
1	100% r.h. at 22°C
2	100% r.h. at 22°C than salt-treatment
3	steam curing at 80°C and 100% r.h.
4	steam curing at 80°C than salt-treatment

The samples of series of 3–4 were steam cured for 3 hrs at 80°C than samples were kept at room temperature (22±3°C) and 100% r.h. Salt-treatment meant to keep the specimens in 10% NaCl solution, between 28 and 38 days (24 hrs in the salt solution, followed by 24 hrs of drying cyclically). Salt-treated samples were kept then at room temperature (22±3°C) and ~100% r.h. after this time. Tests of hardened samples were carried out in ages of 24 hrs, as well as 7, 28, 90 and 180 days. Hydration process was studied by thermal test (DTA/TG/DTG) using Derivatograph Q-1500 D and X-ray diffraction (XRD) using Philips PW 3710 diffractometer. Simultaneous application of thermoanalytical methods and powder diffraction made possible to carry out detailed analysis of phase modifications.

X-ray patterns of salt-treated cements indicated the formation of calcium-aluminate-chloro-hydrate, Friedel's salt ($C_3A \cdot CaCl_2 \cdot H_{10}$). We also studied the influence of steam curing on chloride ion binding capacity of cements. The other Cl⁻-containing hydrate, Kuzel's salt ($C_3A \cdot 0,5CaSO_4 \cdot 0,5CaCl_2 \cdot H_{12}$) did not appear in salt-treated samples [5,10]. The intensity of Friedel's salt was higher in the steam cured samples than those of non-steam cured samples of cements. X-ray patterns indicated formation of monosulphate ($C_3A \cdot 3CaSO_4 \cdot H_{12}$) parallel to ettringite formation ($C_3A \cdot 3CaSO_4 \cdot H_{32}$) in the accelerating cured samples (steam curing at 80°C). The intensity of ettringite was higher in the salt-treated samples compared to the samples kept without salt-treatment. This observation can be explained with the reaction of sulphate ions released by the transformation monosulphate → Friedel's salt. The reaction of sulphate ions and the AFm (aluminate-ferrite mono-) phases lead to the delayed (secondary) ettringite formation.

The most remarkable difference between the results of thermal tests of salt-treated and non salt-treated samples is the presence of a peak at approx. 360°C, which can be attributed to formation of Friedel's salt. About 40% of the water content (4 mole water) of Friedel's salt is lost below 200°C.

Previously the chemically bound chloride content was calculated by Hooton and Titherington (2004) using indirect method where both the total and water soluble chloride content were measured with analytical methods. They found that blast-furnace slag cement pastes have higher chloride ion binding capacity compared with the PC control. This conclusion is in accordance with our test results obtained from the thermogravimetric mass loss of the second dehydration step of Friedel's salt using the TG and DTG curves of thermal tests.

Fig. 1 shows the first derivatives of thermogravimetric curves (DTG curves) in case of non salt-treated (non steam cured, age: 90 days) and salt-treated samples steam cured at 80°C at the age of 180 days.

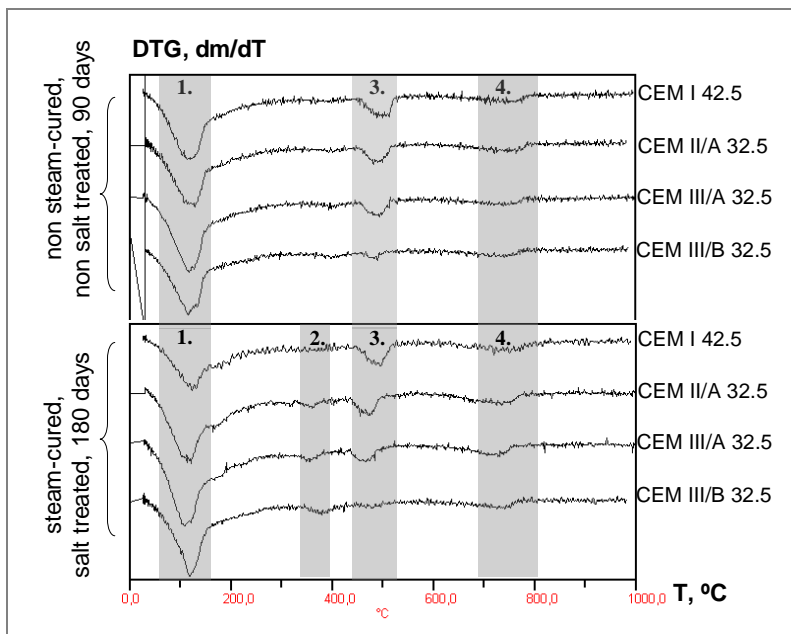


Fig. 1

DTG curves hydrated cement samples; non steam cured samples and non salt-treated samples at the age of 90 days; steam cured then salt-treated samples, at the age of 180 days, salt-treatment between the ages of 28-38 days. Notation: 1. ettringite and humidity; 2. Friedel's salt; 3. portlandite; 4. carbonates and CSH

We calculated the chemically bound chloride content from the second step of dehydration of Friedel's salt. 6 moles of water represent 1 mole of Friedel's salt. The stoichiometric factor calculating the amount of Friedel's salt is $f_{Fs} = 5,2$ (Kopeckó, 2006). The chloride content in Friedel's salt is 12,6%. Fig. 2 shows the diagram of the chemically bound chloride content of salt-treated samples related to the mass of samples without ignition loss.

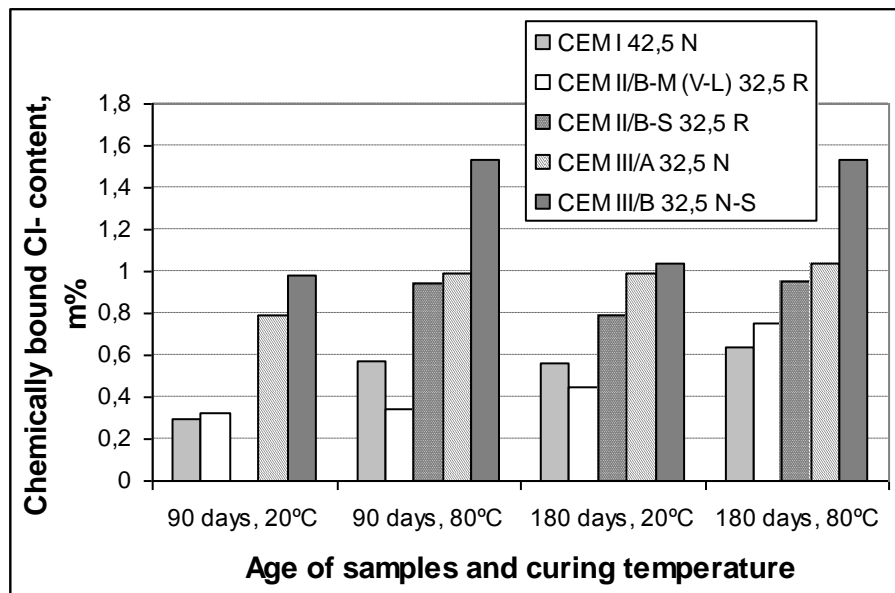


Fig. 2

Amount of chemically bound Cl- ions (m%) related to the mass of samples without ignition loss as functions of ages and curing temperatures

Test results indicated that steam cured cements can bind higher amount of chloride ions than naturally hardened ones. Chloride ion binding capacity of tested cements in decreasing sequence at the age of 180 days was the following: (1) CEM III/B 32.5 (GGBSC); (2) CEM III/A 32.5 (GGBSC); (3) CEM II/A 32.5 (GGBSPC); (4) CEM II/B-M (V-L) 32,5; (5) CEM I 42.5 (OPC).

5. CONCLUSIONS

Corrosion of steel reinforcement starts whenever its passivating layer dissolves. Chloride ions induce electrochemical corrosion in form of pitting corrosion.

Chlorides may be present in concrete from its constituents (like admixtures), from de-icing salts, from seawater or from PVC during fire.

Chemically bound chlorides do not induce corrosion. It is also known since hundred years that C_3A clinkers bind $CaCl_2$ in form of Friedel's salt. However, $NaCl$ of de-icing salts can be only bound by the cement stones if any hydrates decompose.

Tests results indicated that $CaCl_2$ and $NaCl$ will be bound by C_3A and C_4AF clinkers in form of Friedel's salt ($C_3A \cdot CaCl_2 \cdot 10H_2O$, or $C_3F \cdot CaCl_2 \cdot 10H_2O$) independently if $CaCl_2$ and $NaCl$ get into the concrete during mixing or after hardening. Chloride ions bounded chemically by C_3S clinkers were not found.

Large portion of concrete structures is made out of steam cured concrete. Steam curing is a generally used method in the production of precast concrete elements. Increased temperature accelerates the hydration resulting high early strength.

Purpose of our last research was to study the influence of steam curing and the effect of different kind and amount of additives on chloride ion binding capacity of cements. Hydration as well as chloride ion binding mechanisms was investigated by TG/DTG/DTA and XRD. Cements were selected with different replacement level of GGBS as well as with replacement by fly ash and limestone. The hardened samples were cyclically immersed in 10 m% $NaCl$ solution (for 1 day) then kept at 100% relative humidity (for 1 day) between the age of 28 and 38 days, respectively.

Test results indicated that steam cured cements can bind higher amount of chloride ions than naturally hardened ones. Chloride ion binding capacity of tested cements in decreasing sequence at the age of 180 days was the following: (1) CEM III/B 32.5 N-S (GGBSC), (2) CEM III/A 32.5 N (GGBSC); (3) CEM II/B 32.5 R (GGBSPC); (4) CEM II/B-M (V-L) 32,5 R (Composite PC); (5) CEM I 42.5 N (OPC).

6. ACKNOWLEDGEMENTS

Authors wish to thank to the Hungarian Research Found for the financial support of the presented research by Grants OTKA 3000 and OTKA T034467. Authors gratefully acknowledge to Danube-Drava Cement Ltd. supporting the presented last research.

7. LIST OF NOTATIONS

A	= Al_2O_3	H	= H_2O
C	= CaO	C_3A	= $3\text{CaO Al}_2\text{O}_3$
F	= Fe_2O_3	C_3S	= 3CaO SiO_2
S	= SiO_2	C_4AF	= $4\text{CaO Al}_2\text{O}_3 \cdot \text{Fe}_2\text{O}_3$

8. REFERENCES

- Balázs Gy. (1996a), „Concrete and reinforced concrete. History of basics.”, *Academy Press*, Budapest
- Balázs Gy. (1996b), „Concrete and reinforced concrete. History of building construct.”, *Academy Press*, Budapest
- Balázs Gy. (2001), „My excursions in the field of concrete research”, *Academy Press*
- Balázs Gy., Tóth E. (editors) (1997), „Diagnostics of concrete structures, I. Methods of diagnostics”, *Műegyetemi Kiadó*
- Balázs, Gy., Csizmadia, J., Kovács, K. (1997), „Chloride ion binding ability of calcium-aluminate, -ferrite and -silicate phases.”, *Periodica Polytechnica Ser. Civil Engineering*, Technical University of Budapest, Vol 41/2, pp. 147-168.
- Breit, W. (2001), „Kritischer korrosionsauslösender Chloridgehalt. Sachstand und neuere Untersuchungen”, *Betontechnische Berichte*, 1998-2000. Verein Deutscher Zementwerke e.V. Forschungsinstitut der Zementindustrie, pp.145-167.
- Dhir, R. K.; El-Mohr, M. A. K. and Dyer; T. D., „Chloride binding in GGBS concrete”, *Cem. Concr. Res.*, Vol. 26 (12), 1996, pp. 1767-1773.
- Friedel, P. M. (1897), „Sur un Chloro-aluminate de Calcium Hydraté se Maclant par Compression”, *Bulletin Soc. Franc. Minéral*, Vol 19, pp. 122-136.
- Hooton, R. D. and Titherington, M. P., „Chloride Resistance of High-performance Concretes Subjected to Accelerated Curing”, *Cem. Concr. Res.*, Vol. 34, 2004, pp. 1561-1567.
- Kopecskó, K. (2006), „Chloride ion binding capacity of clinker minerals and cements influenced by steam curing”, PhD Thesis, BME, Budapest, pp. 47-49.
- Lukas, W. (1983), „Zur Frage der Chlorid-bindung und der Korrosion von Stahl im Beton”, *Kolloquium Chloridkorrosion*, Wien
- Luo, R.; Cai, Y.; Wang, C. and Huang, X., „A study of chloride binding and diffusion in GGBS concrete”, *Cem. Concr. Res.*, 2003, Vol. 33 (1), pp. 1-7.
- Volkwein, A. (1987), „Chlorideindringen und Stahlkorrosion durch Chlorid”, *Baustoffinstitut der Technischen Universität München*, Fachtagung/1987, pp. 17-22.

Vertical Displacements of a Steel-concrete Superstructure, 51m Long, Under the THALYS Train Load, with Speeds Ranging Between 1...110m/s

A THALYS nagysebességű vonat által gerjesztett lehajlások egy öszvérkeresztmetszetű híd hosszában

Deformații vertical la un pod de cale ferată cu secțiune mixtă având deschiderea de 50m sub acțiunea convoiului THALYS, cu viteze între 1...110m/s

Gavril KÖLLŐ, Mircea A. SUCIU

Railway Bridge Department at the Technical University of Cluj-Napoca, Romania,
Civil Engineering Faculty

ÖSSZEFOGLALÓ

Nagysebességű vasuti pálya esetében, amikor a vonatok 200km/h-nál nagyobb sebességgel közlekednek, feltevődik a kérdés, milyen lehajlások, függőleges mozgások jönnek létre a mozgó szerelvények alatt. Milyenek kéne kialakítani a hídszerkezetet a híd hosszába, milyen geometriájú legyen a sín koronaszintje a szerkezet hosszába?

Ebben a tanulmányban a THALYS nagysebességű vonat tehelése alatt gerjesztett lehajlásokat elemezzük. A maximális lehajlás 23,10mm, ami 252km/h sebesség mellett jön létre, 396km/h sebességnél a lehajlás csak 17,61mm. Minden hídszerkezet esetén a nagysebességű közlekedésnél szükséges a kritikus sebesség meghatározása.

REZUMAT

În cazul podurilor pe care circulația se desfășoară cu viteze mari ($V > 200\text{km/h}$) se pune problema determinării deplasărilor în vederea stabilirii unei contrasăgeții pe pod.

În lucrarea de față sunt analizate deplasările verticale ale tablierului la diferite viteze pentru trenul THALYS și este stabilită o contrasăgeată ținând seama de aceste deplasări. Deplasarea maximă obținută este de 23,10mm care s-a realizat pentru viteza de 252km/h. Pentru 396km/h s-a obținut o deplasare pe verticală de 17,61mm. Pentru fiecare structură de pod la viteze mari este necesară determinarea unei viteze critice, viteză pentru care deplasarea verticală este maximă.

ABSTRACT

The paper analyses the vertical displacements of a railway bridge, steel-concrete composition, 50m span, under the action of a high speed train.

The critical running speed for the analyzed superstructure, train, and speed range is 70m/s (252 km/h). The maximal deflection has been recorded at this speed at mid-span of the superstructure; its value was 23.10mm, higher than the 17.61mm deflection recorded at the speed of 110m/s (396km/h). Given that the amplification of the vibrations can appear also at the common running speeds of the high speed trains, we can state that a dynamic calculation similar to the one we have made here is recommended or even compulsory.

Keywords: bridges, high speed trains, vibrations, vertical displacements.

1. INTRODUCTION

The increase of the running speed on the railway generates in the bridge superstructures the apparition of certain deflections and vibrations that can be amplified under certain conditions. This paper presents a comparative study of the recorded deflections of a railway superstructure that has a horizontal running track under dynamic loads (Thalys train), running at speeds between 1...110m/s (3.6...396km/h).

The objectives are to determine the maximal deflections of the analyzed superstructure for the considered running speeds and to determine the critical speed that has as an effect the amplification of the vibrations and the increase of the deflections.

2. WORK METHOD

A steel-concrete section railway bridge superstructure has been carried into the SAP2000 finite element calculation programme.

The 51m superstructure featured in Fig. 1 has been divided and carried into the SAP2000 finite element calculation programme considering elements of 0.5m along the bridge. Thus, 103 characteristic sections have been obtained.

The analyzed superstructure is made up of "shell" plane elements, the rails and the linear elements of the sidewalks have been inserted as "frame" rod type elements, the concrete slab the rails are fixed into has been inserted as "solid" type elements.

Thalys is a high speed train made up of 2 engines and 8 intermediary cars, with axle loads between 7.25 and 8.5 tons, the distance between the car bogies of 18.7m. The total length of the train is $L_{conv}=193.14m$.

From the moment the first axle enters the superstructure until the last axle leaves the superstructure, the train covers 102 0.5m-long elements and has 490 successive loading steps.

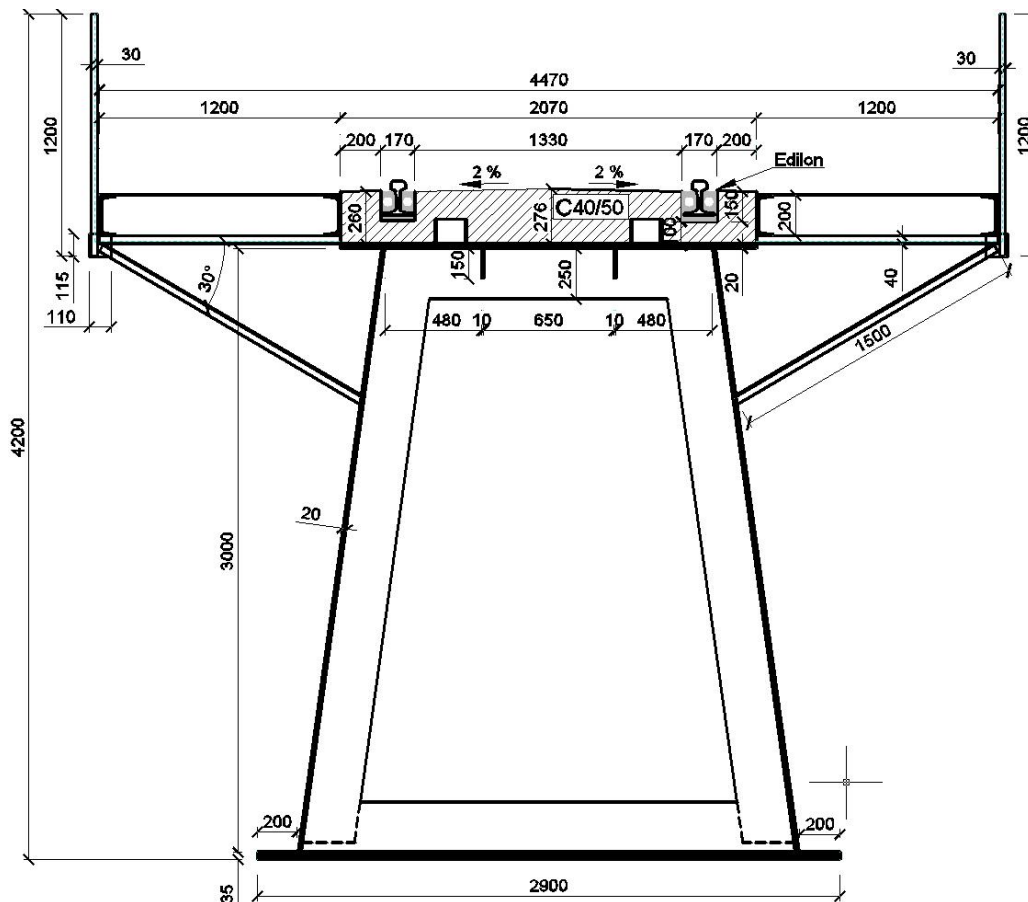


Fig. 1.
Cross section of the superstructure.

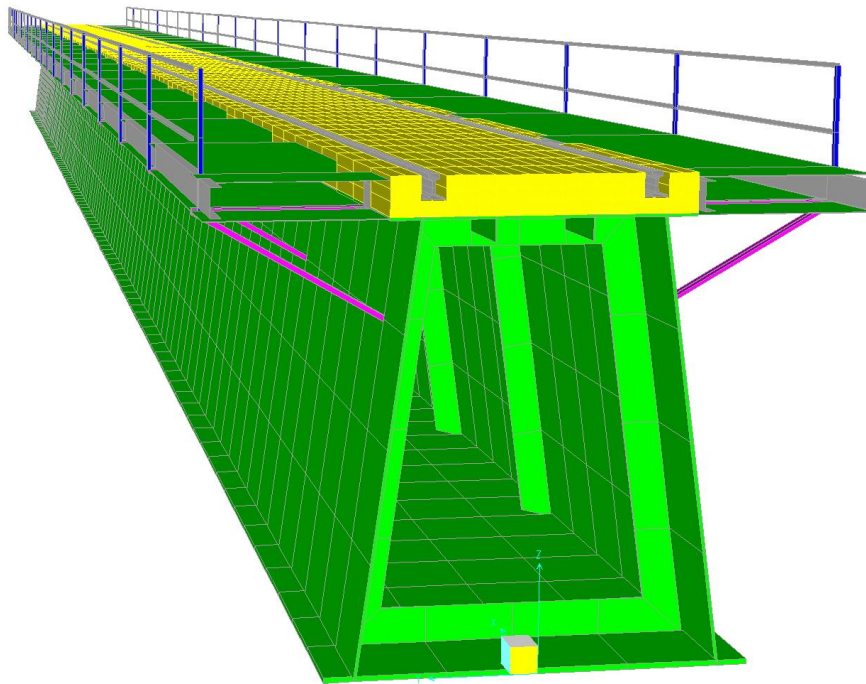


Fig. 2.
The structure analysed with the SAP2000 programme

The vertical deflections of the superstructure have been recorded at the level of the rails, for all the 490 loading steps. The dynamic analyses are non-linear and they have been made using the direct integration method, with a 5% damping coefficient, directly proportional with the weight. The deflections obtained in 3 of the 103 characteristic sections, namely the ones situated at $L/4$, $L/2$, and $3L/4$, are represented in the graphics below.

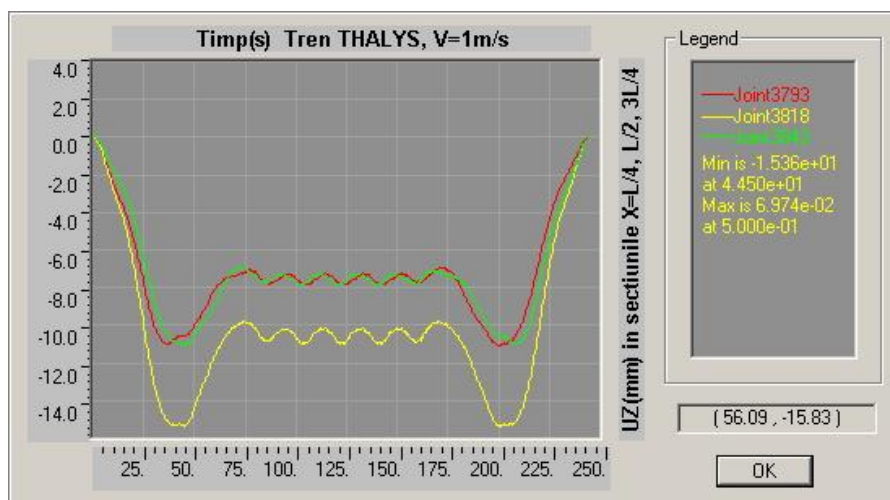


Fig. 3.
Deflections $UZ(mm)$, Thalys, $V=1m/s$ (3.6km/h)

We notice that at the speed of $1m/s$ the maximum value of the recorded deflection of the superstructure is $15.36mm$. The superstructure is loaded and the results are recorded for 245 seconds, the time needed by the train to cover the $51m$ -long superstructure with the speed $V=1m/s$.

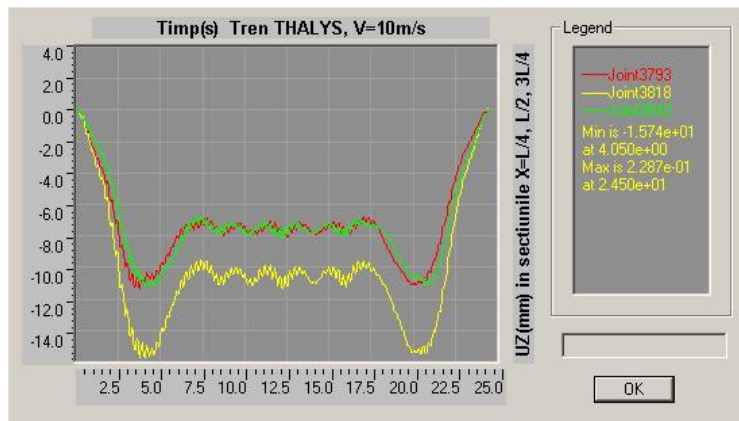


Fig. 4.
Deflections $UZ(mm)$, Thalys, $V=10m/s$ (36km/h)

We notice that at the speed $V=10m/s$ vibrations start to appear in the superstructure.

The superstructure is loaded and the results are recorded for 24.5 seconds, the time needed by the train to cover the 51m-long superstructure with the speed $V=10m/s$. The maximum value of the recorded deflection at $L/2$ is 15.74mm.

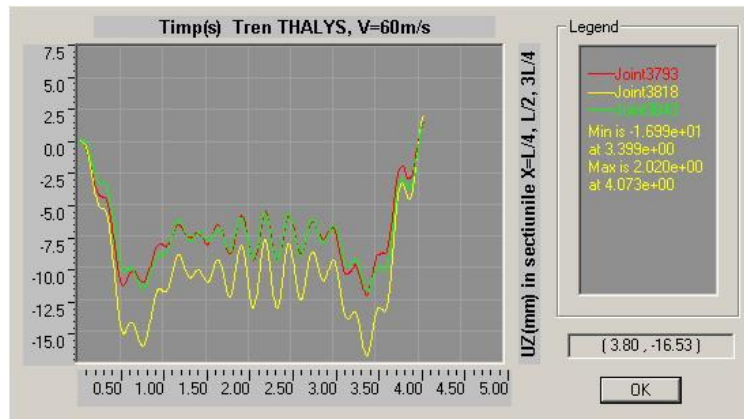


Fig. 5.
Deflections $UZ(mm)$, Thalys, $V=60m/s$ (216km/h)

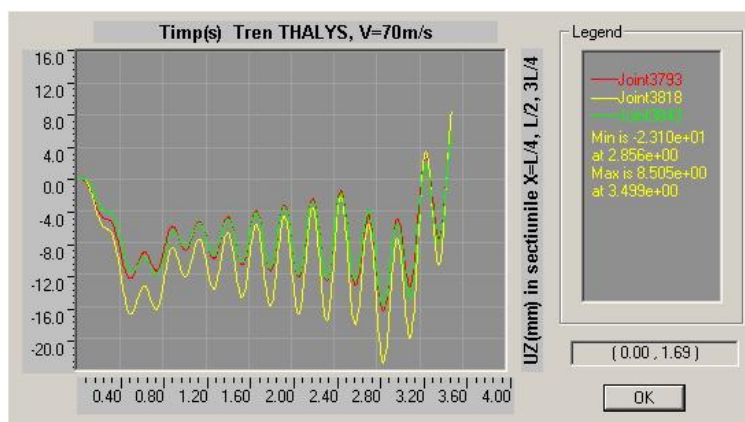


Fig. 6.
Deflections $UZ(mm)$, Thalys, $V=70m/s$ (252km/h)

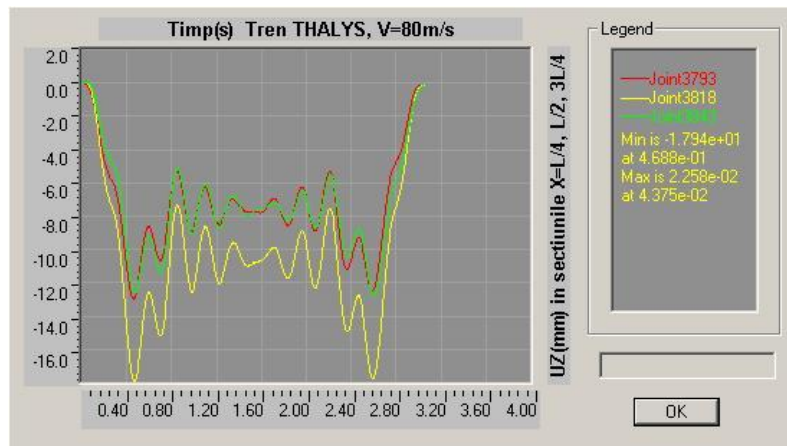


Fig. 7.
Deflections UZ(mm), Thalys, V=80m/s (288km/h)

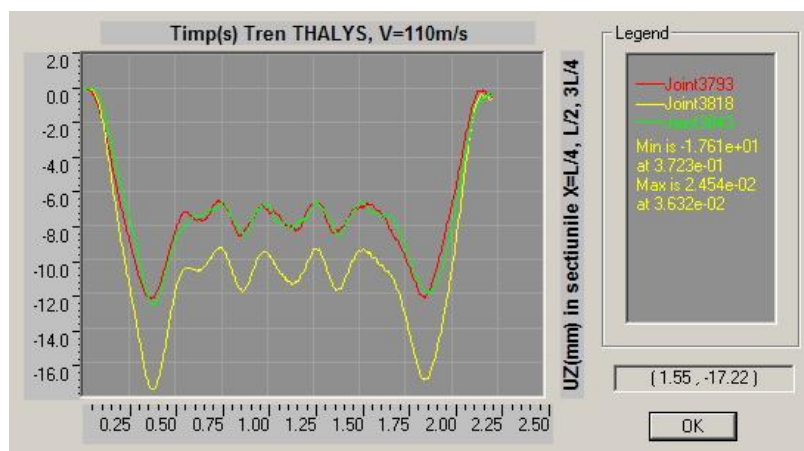


Fig. 8.
Deflections UZ(mm), Thalys, V=110m/s (396km/h)

Tab. 1. Deflections recorded with SAP2000 programme.

THALYS train speed	Maximal and average deflections UZ (mm) measured in the L/4, L/2, and 3L/4 sections						Maximal rail deflections, Afferent section, average maximal rail deflec- tions (mm) throughout the loading time		
	X=L/4 (13m)		X=L/2 (25.5m)		X=3L/4 (38.0m)		UZ(-) max (7)	X (m) (8)	UZ(-) avg. (9)
	UZ(-) max (1)	UZ(-) avg. (2)	UZ(-) max (3)	UZ(-) avg. (4)	UZ(-) max (5)	UZ(-) avg. (6)			
1m/s (3.6)	11.07	7.25	15.36	10.12	11.06	7.25	15.38	24.5	9.67
10 (36)	11.33	7.25	15.74	10.12	11.23	7.25	15.74	26.0	9.86
20 (72)	11.08	7.25	15.40	10.12	11.12	7.25	15.42	24.5	9.70
30 (108)	11.53	7.23	15.98	10.09	11.40	7.23	15.98	25.0	10.03
40 (144)	11.43	7.25	15.81	10.12	11.41	7.25	15.81	25.0	9.95
50 (180)	11.57	7.25	16.24	10.11	11.51	7.25	16.26	24.5	10.11
60 (216)	12.25	7.25	16.99	10.11	11.86	7.25	16.99	25.0	10.55
70 (252)	16.57	7.28	23.10	10.16	16.04	7.28	23.10	25.0	14.33
80 (288)	12.96	7.25	17.94	10.12	12.83	7.25	17.94	25.0	11.21
90 (324)	13.03	7.25	18.21	10.12	12.90	7.25	18.21	25.5	11.32
100 (360)	13.15	7.23	18.13	10.09	12.83	7.23	18.16	24.5	11.33
110 (396)	12.28	7.26	17.61	10.13	12.62	7.26	17.61	26.0	10.92

In the presented graphics we notice that at the speed of 70m/s (252km/h) a phenomenon of amplification of the vibrations is recorded, the maximal recorded deflection of the superstructure being 23.10mm. At the speed of 110m/s (396km/h) the analyzed superstructure has a much better behaviour, the amplitude of the vibrations decreases, the maximal deflection is 17.61mm.

The significance of the values in the table:

- for a certain running speed, the SAP2000 programme records in all the 103 characteristic sections of the superstructure all the deflections that occur in the 490 load steps with the Thalys train;
- out of all these sections we have selected the ones from L/2, L/4, and 3L/4 and out of the 490 values recorded in these three sections under loads we have selected only the maximal deflections, inserted in columns (1), (3) and (5);
- for the three analysed sections we have made the arithmetical average of the 490 values of the deflections recorded in the 490 loading steps (all throughout the time when axles of the train are present on the superstructure) inserted in the table in col. (2), (4) and (6);
- for each running speed, the highest deflection recorded in the superstructure at the level of the rail is given in col. (7), the section where it was recorded is given in col. (8), and the average of all the maximal deflections recorded in all the 103 sections is inserted in col. (9);
- the sign (-) that appears near U_z means that all the deflections in that column are below the horizontal line of the track in the absence of the train;

3. OBSERVATIONS AND CONCLUSIONS

1) A first observation regarding the values in the table refers to the value of the maximal deflections that have been recorded. We notice that the critical running speed for the analyzed superstructure, train, and speed range is 70m/s (252 km/h). The maximal deflection has been recorded at this speed at the middle of the superstructure; its value was 23.10mm, higher than the 17.61mm deflection recorded at the speed of 110m/s (396km/h). Given that the amplification of the vibrations can appear also at the common running speeds of the high speed trains, we can state that a dynamic calculation similar is recommended.

2) Based on a calculation similar to the one we have presented here, the critical speeds that have as an effect the amplification of the vibrations can be pointed out. Afterwards the designer will find through several attempts the critical speed (for this particular case, the attempts with 69m/s, 71m/s, etc., speeds around 70m/s, as shown in the table).

3) Another observation based on the analysis of the values in this table refers to the variation of the average deflections. This table shows that in the L/4, L/2 and 3L/4 sections, the average values of the deflections recorded in the rail vary insignificantly in relation with the speed of the train (the average values of the recorded deflections in the middle of the superstructure vary between 10.12mm for $V=1\text{m/s}$ and 10.13mm for $V=110\text{m/s}$, the maximal value being 10.16mm for $V=70\text{m/s}$).

This fact allows us to state that regardless of the speed of the train, the bridge records vibrations that are close to an average deflection for all the sections of the beam. Based on the average values of the deflections recorded at mid-span with a straight running track, the designer can suggest more shapes of counter deflection to be studied (parabolic, linear side ramps with circular curve in the central area, etc.) so that the maximal value of the designed counter deflection will be around 10...12 mm.

REFERENCES

- [1.] C. Esveld: *Modern Railway Track*, MRT-Productions, ISBN 0-800324-1-7,1989.
- [2.] C. Esveld, A.W.M. Kok,: *Dynamic Behavior of Railway Track*, Railway Engineering Course TU Delft, Department of Civil Engineering, November 1996.

Vertical Displacements of a Steel-concrete Railway Superstructure, 51m Long, Under the 250kN Mobile Axle Load, for Speed Ranging Between 1...150m/s.

Egy nagysebességű mozgó tengely (P=250kN) által gerjesztett lehajlások
egy öszvérkeresztmetszetű híd hosszában

Deformații vertical la un pod de cale ferată cu secțiune mixtă
având deschiderea de 50m sub acțiunea unei osi mobile (P=250kN),
cu viteze între 1...150m/s

Mircea A. SUCIU, Gavril KÖLLŐ

Railway Bridge Department at the Technical University of Cluj-Napoca, Romania,
Civil Engineering Faculty

ÖSSZEFOGLALÓ

Nagysebességű vonatok által gerjesztett lehajlások jobb megértéséhez ebben a tanulmányban egy P=250kN tengelyterhelésű különböző nagysebességgel áthaladó erőpár hatását tanulmányozzuk. A szerkezet hossza 51m, fesztávolsága 50m. A tanulmány célja a szerkezet viselkedésének a tanulmányozása egy tengelyterhelés dinamikus hatására.

REZUMAT

Pentru a înțelege comportarea unui suprastructuri de 51m lungime (50m deschidere) la acțiunea convoaielor de mare viteză este necesară într-o primă fază determinarea răspunsului dinamic din încărcarea cu o osie mobilă. Încărcarea cu osia mobilă P=250kN a modelului considerat s-a efectuat pentru a se putea face observații asupra răspunsului în deplasări ale tablierului la viteze care depășesc viteze curente atinse în prezent.

ABSTRACT

The paper analyses the vertical displacements of a railway bridge superstructure, steel-concrete composition, 50m span, under the the 250kN mobile axle load. The running track of the bridge has a special structure: the rails are continuously fixed into the concrete slab using the Edilon corkelast material.

In order to determine the impact of the increased speed upon the vibrations and deflections of a mixed section railway bridge superstructure, this superstructure has been carried into the SAP2000 finite element calculation programme. Sixteen non-linear dynamic analyses have been performed with the 250 KN mobile axle that covers the analysed model with speeds from 1, 10, 20, 30... 150m/s (3.6...540km/h).

Based on the results presented in this paper, we can say that, for the high speed trains that run at a speed that is close to 60m/s on this superstructure, it is possible that the vibrations and vertical deflections will be amplified. This amplification will be reached if the frequency with which the axles of the train get to L/2 is close to the own frequency of the first vibration mode of the analysed structure.

Keywords: bridges, high speed trains, vibrations, vertical displacements.

1. INTRODUCTION

In order to understand the behaviour of a superstructure under the action of high speed trains, first we need to determine the dynamic answer to the load of one mobile axle. The load with the 250kN mobile axle

of the considered model has been chosen in order to be able to make observations regarding the superstructure displacement answer to speeds exceeding the common speeds presently reached on the Romanian railways.

The objectives are to determine the influence of the increased speed of the mobile axle upon the vibrations and deflections recorded in the analysed superstructure.

2. WORK METHOD

In order to determine the impact of the increased speed upon the vibrations and deflections of a mixed section railway bridge superstructure, with a 50m span and the cross section as seen in Fig. 1, this superstructure has been carried into the SAP2000 finite element calculation programme.

It is important to know the deflections recorded under the action of a mobile axle, in the dynamic analyses for regular or high speed trains, because the second axle of the train will follow a path that has been deformed by the first axle.

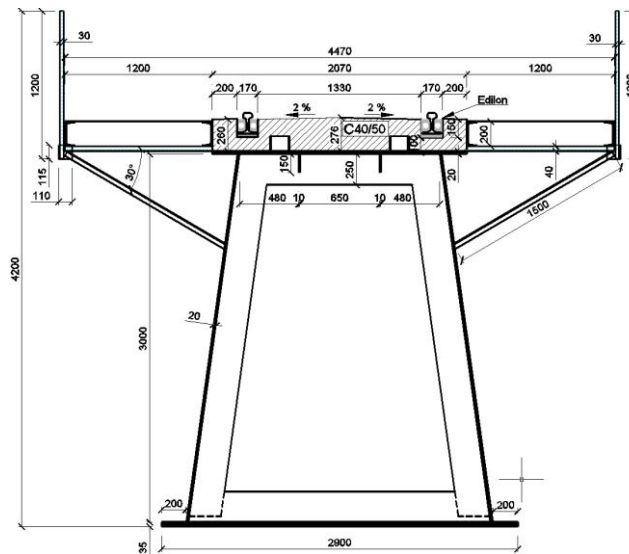


Fig. 1.
Cross section of the superstructure

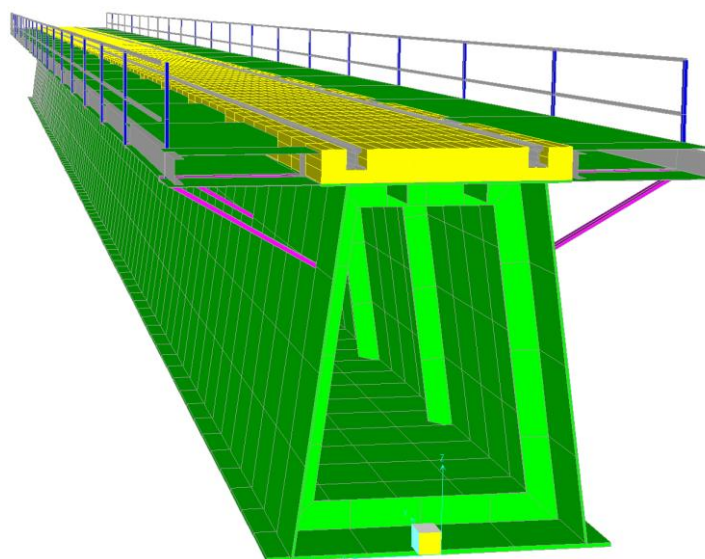


Fig. 2.
The structure analysed with the SAP2000 programme

In order to obtain results that are as close to reality as possible, we have considered a space moulding of the structure was necessary, with all the comprised elements, instead of making the analysis for a free beam having an equivalent rigidity.

The box section and the sidewalk panes are made of “shell” plane elements, the rails and the linear elements of the sidewalks have been inserted as “frame” rod type elements, the concrete slab the rails are fixed into has been inserted as “solid” type elements.

The analysed superstructure is 51m-long and it has been divided into 0.5m-long elements along the way, obtaining 103 characteristic sections. The dynamic analyses have been made considering the $P=250\text{KN}$ constant force, charging the structure in 104 load steps. The vertical deflections of the superstructure have been recorded at the rail level, for all of the 104 load steps. The dynamic analyses have been made using the direct integration method. The vertical deflections in 3 sections, at $L/4$, $L/2$, and $3L/4$, are represented in the graphics below.

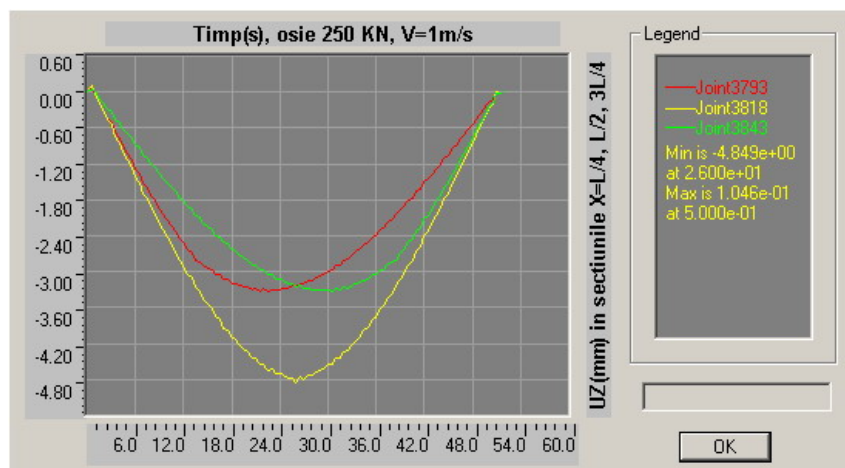


Fig. 3.
Vertical deflections $UZ(\text{mm})$, $P=250\text{KN}$, $V=1\text{m/s}$ (3.6km/h)

We notice that at the speed of 1m/s the vibrations are almost inexistent. The maximum deflection of the superstructure is 4.849mm and it is reached in the $L/2$ section, at second 26.

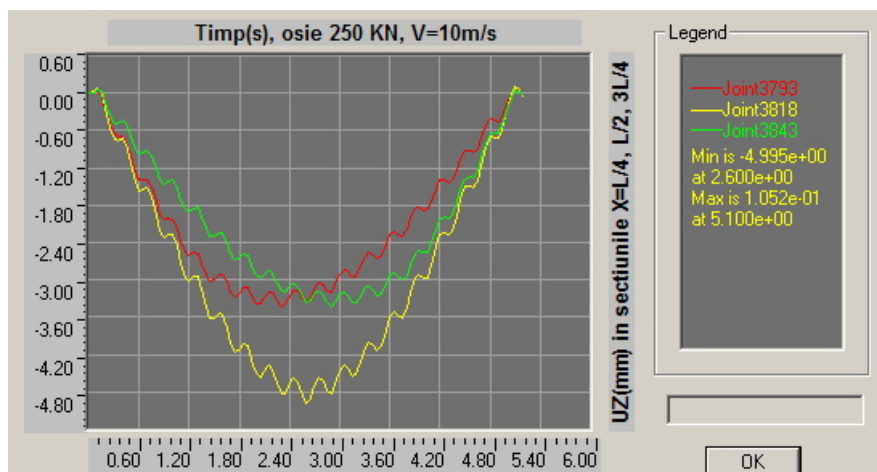


Fig. 4.
Vertical deflections $UZ(\text{mm})$, $P=250\text{KN}$, $V=10\text{m/s}$ (36km/h)

At $V=10\text{m/s}$ vibrations start to appear in the superstructure. The superstructure is loaded for 5.1s , the maximum value of the recorded deflection at $L/2$ is 4.995mm .

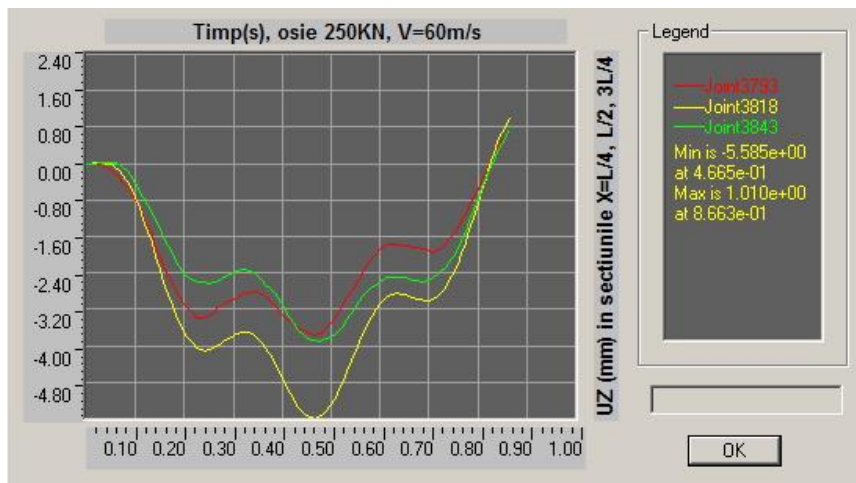


Fig. 5.
Vertical deflections $UZ(mm)$, $P=250KN$, $V=60m/s$ (216km/h)

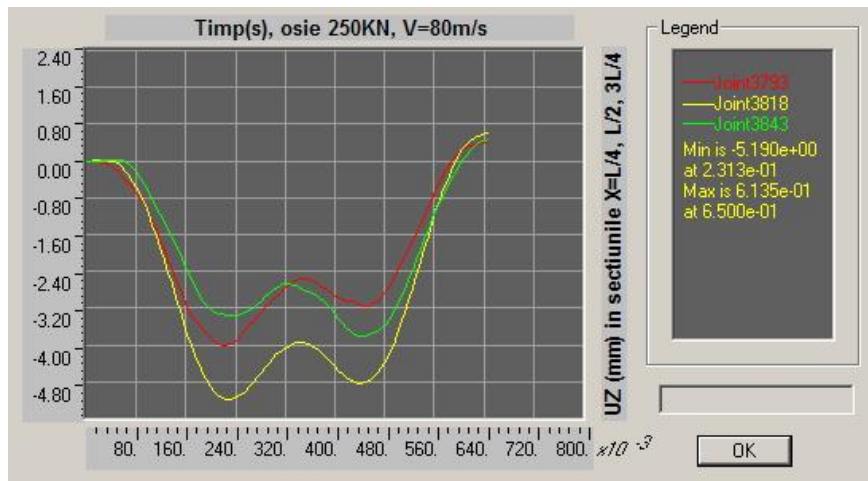


Fig. 6.
Vertical deflections $UZ(mm)$, $P=250KN$, $V=80m/s$ (288km/h)

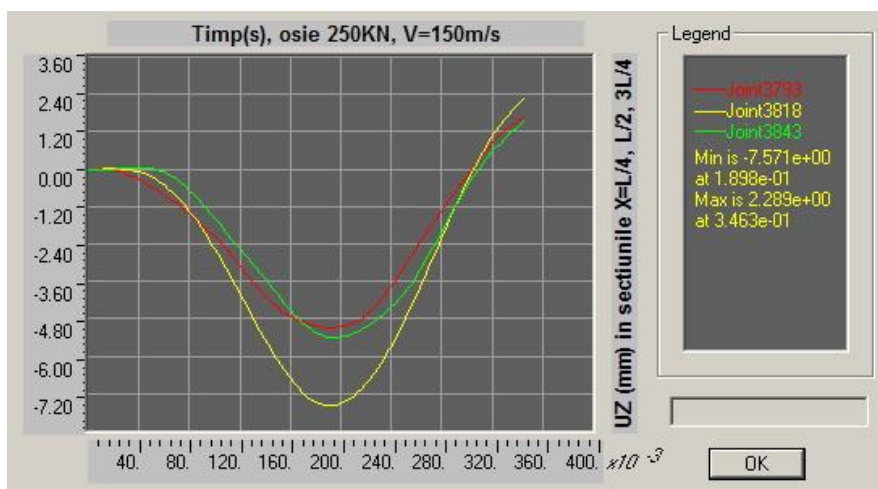


Fig. 7.
Vertical deflections $UZ(mm)$, $P=250KN$, $V=150m/s$ (540km/h)

OBSERVATIONS

The featured graphics allow us to notice that, as the speed increases from 1 to 150 m/s, the time needed to cover the 51m-long superstructure decreases from 51 seconds to 0.34s and the amplitude of the vibrations increases. However, the maximum reached deflections of the superstructure do not compulsorily grow together with the increase of the speed. They are influenced by the vertical position of the mid-span section within the current oscillation. Thus, if the moment the axle gets near the mid-span this section is in a position of minimum of the current oscillation, then the deflection is maximal and it is obtained from static load (that can be considered the maximal value obtained at $V=1\text{m/s}$, where no vibrations have been recorded) to which we add the deflection difference of the current oscillation.

We notice that the deflections recorded in the $L/4$, $L/2$, and $3L/4$ sections normally grow together with the increase of the speed, but there are also speeds for which the maximum deflections obtained are lower than the ones recorded at inferior speeds. The section where the maximal deflections have been obtained is near the mid-span section, but it is not compulsory that it be in this section.

Tab. 1. Results obtained in the dynamic analyses made with the 250KN mobile axle that covers the 51m-long superstructure, with speeds ranging from 1-150m/s (3.6-540km/h).

The speed of the mobile axle $P=250\text{KN}$	Maximal deflections UZ (mm) measured in the $L/4$, $L/2$, and $3L/4$ sections and the position of the axle on the bridge (the covered distance) the moment the maximal value is recorded.						Maximal deflections measured in the rail, the covered distance and the section where the maximal value was recorded.		
	$X=L/4$ (13m)		$X=L/2$ (25.5m)		$X=3L/4$ (38m)				
	V m/s (v km/h)	UZ(-) mm	Dist m	UZ(-) mm	Dist m	UZ- mm	Dist m	UZ(-) mm	Dist m
1m/s (3.6)	3.33	22.5	4.85	26.0	3.32	30.5	4.85	26.0	25.5
10 (36)	3.43	23.0	5.00	26.0	3.43	29.0	5.00	26.0	25.5
20 (72)	3.49	21.0	5.09	26.0	3.48	31.5	5.10	26.5	26.0
30 (108)	3.59	22.5	5.07	23.0	3.61	30.5	5.09	23.0	22.5
40 (144)	3.65	20.0	5.16	29.5	3.70	29.5	5.19	29.0	28.5
50 (180)	3.82	24.0	5.42	24.0	3.62	24.5	5.47	24.5	24.0
60 (216)	3.77	28.0	5.58	28.0	3.89	28.5	5.62	28.0	27.5
70 (252)	3.72	16.0	5.34	31.5	3.97	32.0	5.38	31.5	27.5
80 (288)	4.02	18.0	5.19	18.5	3.81	35.5	5.24	18.0	23.0
90 (324)	4.26	20.0	5.68	20.0	3.71	20.5	5.72	20.0	23.5
100 (360)	4.47	21.5	6.11	21.5	4.04	22.5	6.14	21.5	24.0
110 (396)	4.64	23.0	6.51	23.5	4.36	23.5	6.54	23.5	23.0
120 (432)	4.79	25.0	6.86	25.0	4.65	24.5	6.90	25.0	24.5
130 (468)	4.90	26.5	7.20	26.0	4.93	26.0	7.20	26.0	25.5
140 (504)	5.00	28.0	7.39	27.5	5.18	28.0	7.43	27.5	27.0
150 (540)	5.08	29.5	7.57	28.5	5.42	29.0	7.59	28.5	26.5

CONCLUSIONS

Based on the results presented in this paper, we can say that, for the high speed trains that run at a speed that is close to 60m/s on this superstructure, it is possible that the vibrations and vertical deflections will be amplified. This amplification will be reached if the frequency with which the axles of the train get to $L/2$ is close to the own frequency of the first vibration mode of the analysed structure.

The maximal deflection in the case of the analyzed superstructure is 7.59mm. This value has been reached for the speed of 150m/s (540km/h) the moment the axle had covered 28.5 of the 51m (it has been recorded in the section placed at 26.5m from the first joint).

The increase of the running speed of the mobile axle determines the increase of the amplitude of the vibrations, but this does not necessarily lead to a continuous increase of the recorded deflections of the superstructure, Fig. 8.

The behaviour of the analyzed model from the point of view of the vibrations and of the deflection pattern corresponds to the known theoretical models.

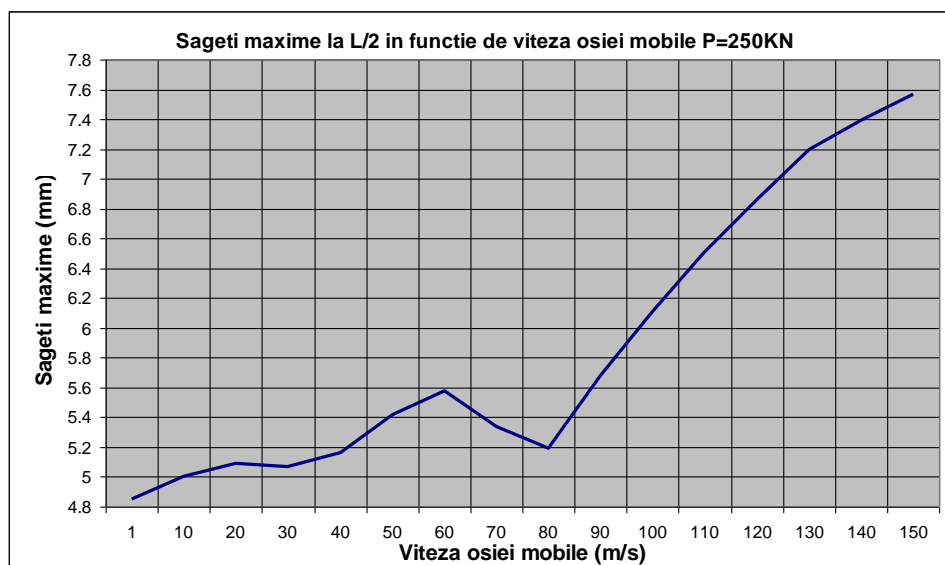


Fig. 8.

/Vertical deflections(mm) recorded at the track level, mid-span of superstructure, for a 250KN mobile axle, speeds $V=1 \dots 150\text{m/s}$ ($3.6 \dots 540\text{km/h}$)

The data offered by this paper are of interest because the second axle of the train will enter the superstructure on a deformed path that records vibrations similar to the ones featured by the graphics Fig. 3 - Fig. 7, according to the running speed.

REFERENCES

- [1.] C. Esvelde: *Modern Railway Track*, MRT-Productions, ISBN 0-800324-1-7,1989.
- [2.] C. Esvelde, A.W.M. Kok,: *Dynamic Behavior of Railway Track*, Railway Engineering Course TU Delft, Department of Civil Engineering, November 1996.